ROSE BENGAL-CONJUGATED GOLD NANOPARTICLES: QUANTIFICATION OF SINGLET OXYGEN GENERATION IN PHOTODYNAMIC THERAPY

By

Manoj Badrinath Kale

A THESIS SUBMITTED TO MACQUARIE UNIVERSITY
FOR THE DEGREE OF MASTER OF RESEARCH
DEPARTMENT OF PHYSICS AND ASTRONOMY
OCTOBER 2016

MACQUARIE
University
SYDNEY·AUSTRALIA

EXAMINER'S COPY

Except where acknowledged in a customary manner, the material presented in this thesis is, to the best of my knowledge, original and has not been submitted in whole or part for a degree in any university.

Manoj Badrinath Kale

Acknowledgements

First, I would like express my deep sense of gratitude to my supervisor, Professor Ewa M. Goldys, who supported me throughout this project. None of this would have been possible without her support.

I am also thankful to the admirable staff in the department of physics and astronomy for their pleasing support.

I wish to thank Macquarie University and ARC Centre of Excellence for Nanoscale BioPhotonics for providing me financial assistance to attend the conference.

I am also thankful to my family for their love and support throughout this project and my life.

Last but not the least, I want to thank my friends, specially Sandhya Clement, for their support and guidance.

List of Publications

- Manoj B Kale, Sandhya Clement, Ewa M. Goldys, "*The comparative study of singlet oxygen generation efficiency of Rose Bengal, Gold nanoparticles, and Gold-Rose Bengal conjugate in photodynamic therapy*." (Presented a poster at SPIE Biophotonics Australasia Conference, Adelaide, Australia- October 2016).

  ** *This work is awarded an ARC Centre of Excellence for Nanoscale BioPhotonics (CNBP) bursary covering registration fee and travel expenses to attend SPIE Biophotonics conference.* **

Abstract

Photodynamic therapy (PDT) is an advanced novel methodology for the treatment of cancers using photosensitizers (PSs) which upon irradiating light generate cytotoxic singlet oxygen ($^1O_2$) and kills cancer cells. The utilization of photosensitizers has some restrictions, like low coefficient of extinction, low $^1O_2$ generation efficiency and cannot be used for treating deep-seated tumours. Nanoparticles (NPs) have various properties that can be applied in PDT to overcome the limitations of PSs.

The main aim of this work is, therefore, to enhance the $^1O_2$ generation efficiency of the photosensitizer Rose Bengal (RB) by conjugating it with the Gold nanoparticles (AuNPs). The quantitative measurement of $^1O_2$ generation is carried out on photosensitizer RB, AuNPs, and Au-NPs conjugated RB (AuRB). The fluorescence probe Singlet Oxygen Sensor Green (SOSG) was used to detect the $^1O_2$. In a systemic study, the dependence of fluorescence on AuRB conjugation with different PS concentrations and the light-irradiation time for $^1O_2$ generation are performed. Finally, the singlet oxygen quantum yield (SOQY) measurements are carried from the calculation of the rate of reaction and discussed. The results of the project state the improvement in $^1O_2$ generation efficiency of PS on conjugation with the NPs.

The successful NP-PS conjugation and high SOQY give the motivation for further studies on the development of the new photosensitizer drugs to treat the cancer cells.

List of Figures

List of Tables

1 Introduction

1.1 Photodynamic therapy

Photodynamic therapy (PDT) is one of several clinically approved treatments for cancer disease. The photosensitizer, the sensitisation light and molecular oxygen present in the tissue play a major role in PDT. PDT depends on the successful delivery of photosensitizers to the tumour tissue and then irradiation with light of appropriate wavelength. The photosensitizer molecules excite upon light absorption and then release the energy. The molecular oxygen present in the tissue absorb this released energy and form reactive oxygen species (ROS) and singlet oxygen ($^1O_2$). The ROS and $^1O_2$ cause permanent damage to the cancer cells.

In recent years, much research has been done towards the advancement and clinical applications of PDT. As the photosensitizers play a vital role in the application of PDT, it has drawn attention for the synthesis and development has been intensely investigated. The clinically approved photosensitizers such as porphyrin- and chlorine- derivatives Photofrin®, Foscan®, Visudyne® have shown outstanding medical outcomes for some cancer treatment [1]. However, the problems such as hydrophobicity of photosensitizers, their high dark toxicity, minimal tumour selectivity and low $^1O_2$ quantum yield of photosensitizers limit the full potential of PDT.

1.2 Motivation of research

The conventional cancer treatment therapies such as chemotherapy, radiotherapy, surgery have a prolonged effect on patient's health such as loss of immunity, hair loss, weight loss, pregnancy complications, nausea. However, PDT does not have the above stated adverse effect on patient's health as it mostly targets specific cancer treatment therapy. For the PDT to be a non-invasive and efficient therapy for oncological diseases, the photosensitizers (1) must be target specific, (2) should not sensitise in absence of light, (3) must be hydrophilic in nature if delivered via bloodstream, (4)

biocompatible, and (5) must have high $^1O_2$ generation efficiency [2]. Even the very efficient and widely used photosensitizer drug Photofrin has the disadvantage of poor target specificity, low solubility in water, long term skin sensitivity [3].

The above problems of photosensitizers motivated us to develop and investigate new photosensitizer-nanoparticle construct. The nanoparticles in combination with photosensitizers can help to overcome the limitations of photosensitizers. The nanoparticles can be used as the delivery vehicle to localize the photosensitizer into the specific tumour and assist in improving the photosensitizer drug efficiency. Also, nanoparticles with their hydrophilic nature can improve the blood circulation time of photosensitizers. Metal nanoparticles such as gold, silver, platinum show plasmonic nature on light irradiation. Gold nanoparticles have advantages of simple synthesis methods, easy surface functionalization; they are available in various sizes and shapes. The optical properties and biocompatibility of gold nanoparticles make them an ideal element for photosensitizer conjugation. The photosensitization effect of the photosensitizer is a result of $^1O_2$ generated. The $^1O_2$ generation efficiency can be improved with the help of the optical property such as surface plasmon resonance. The plasmon resonance can enhance the electric field near the photosensitizer molecule thus contributing in generating the $^1O_2$ from the photosensitizer molecule. This property of gold nanoparticles inspired us to carry out this project.

Finally, we are inspired to select RB as a photosensitizer molecule by its specific features and clinical importance. The RB is hydrophilic in nature and has high singlet oxygen quantum yield in water (0.76) compared to other PS make it potential candidate for use in PDT [4]. The hydrophilic nature of RB results in low intracellular uptake which leads to the low tumour penetration. However, chemical conjugation of RB with AuNPs may increase the intracellular uptake.

1.3 Research framework and objectives

This nine-month Master of Research project has been initiated in January 2015 and has been accomplished within the Department of Physics and Astronomy, Faculty of Science and Engineering at Macquarie University in Sydney, Australia. Based on Macquarie University's guidelines, the main body of this thesis must not exceed 50 pages.

The main objectives of this research work were:

(1) To synthesize the gold nanoparticles (AuNPs) of uniform size and shape.

(2) To modify the surface of the AuNPs by attaching functional groups to enhance conjugation with different concentrations of Rose Bengal photosensitizer.

(3) To characterize the synthesized compounds and intermediates to confirm the precise structure and purity.

(4) To carry out the photo-physical experiments on AuNPs, AuRB conjugate to detect and measure the singlet oxygen quantum yield by using a singlet oxygen sensor green probe.

(5) To compare the singlet oxygen generated by AuNPs and AuRB with the reference photosensitizer and to evaluate the efficiency of the newly formed complex conjugate as a potential drug in photodynamic therapy.

1.4 Thesis overview and contributions

This thesis consists of five chapters. The first chapter includes this introduction while the second chapter covers the essential background in the photodynamic therapy field.

In chapter 3, the characterization instruments and methods used are explained. The theoretical background and working principle of fluorescence spectrometer, UV-Visible spectrometer and diffused light spectrometer are discussed. Furthermore, singlet oxygen generation and detection techniques are explained.

Chapter 4 contains main experimental results with the discussion. In the beginning, the various chemicals used and the synthesis methods of Au nanoparticles and AuRB conjugation are explained. Then, to confirm the successful synthesis of the Au nanoparticles and AuRB conjugation the characterization results of the UV-Visible absorption spectrum. Also, diffused light spectrum measurements for size and surface charge potential are discussed. Next, the photobleaching effect on RB, AuNPs, AuRB conjugate is explained with the help of fluorescence spectroscopy. The singlet oxygen generation mechanism is explained. To detect the singlet oxygen generated by photosensitizer bleaching, the singlet oxygen sensor green probe (SOSG) is used. Moreover, then from the fluorescence intensity curve and UV-Visible absorption values of AuNPs and AuRB and by taking singlet oxygen quantum yield of RB as a reference value, the amount of singlet oxygen produced them calculated. Finally, the SOQY of nanoparticles and photosensitizers are compared and discussed.

Finally, this thesis closes with a conclusion and a description of future work.

2 Photodynamic therapy background

This chapter will introduce the basic working principle of photodynamic therapy. In addition, the advantages and limitation of various photosensitizers will be presented. Finally, this chapter gives the literature overview on different nanomaterials that are used in photodynamic therapy.

2.1 Introduction of photodynamic therapy

Light has been used in medical treatment for thousands of years [5]. The first application of PDT in the treatment of skin related diseases began in the nineteenth century [6]. The mechanism of its action came into the picture with work of Oscar Raab, and his supervisor Von Tappeiner who noticed acridine in the presence of light killed a single cell eukaryotes organism called Paramecium [7]. The core mechanism of PDT involves the localization of photosensitizer (PS) drug near cancer affected tissue followed by the irradiation of the light of appropriate wavelength for PS activation. The sensitized PS molecules which activate and transfer energy to surrounding molecular oxygen. This molecular oxygen creates the reactive oxygen species (ROS) including singlet oxygen ($^1O_2$) which kills the targeting cells [8-10]. The aim of this project is the enhancement of the photodynamic action of a photosensitizer drug by conjugating it with nanoparticles as carrier agents. The photodynamic action is increased by improving the $^1O_2$ generation efficiency of the PDT drug. This efficiency is represented in terms of singlet oxygen quantum yield (SOQY).

PDT is more advantageous compared to the conventional therapeutic methods because of low intrusiveness, low toxicity, better treatment results, minimizing after treatment sickness and increased chances of the life survival chances of patients [11]. For the last three decades, PDT has been used in

the treatment of many skin cancers [12], bladder cancer [11], and early stage lung cancer [13]. Despite intensive research, the application of PDT in cancer therapy remains limited. There are still some limitations that are needed to overcome such as appropriate choice of PS, suitable tissue penetration depth, maximum light wavelength, long-term cell response after treatment. Scientists and academicians are trying to improve the applicability of PDT by making new PS formulations combining the PS with nanomaterials and biomaterials. Biomedical research on PDT application in oncological treatment is also going on.

Figure 2.1 shows how tumour cells respond to the photosensitizer drugs in PDT. After light absorption, the PS produces $^1O_2$ which initiate necrosis, apoptosis and damage of tumour cells. The necrosis and apoptosis cause the generation of heat-shock protiens 70 (HSP70). HPS70 stops the destruction of tumour cells by necrosis and apoptosis by generating antigents to debdritic cells that travel to lumph node [14]. The matured DCs attracted by cytokines are then released at the lymph nodes and produce antigens against T lymphocytes. The T lymphocytes turn into T cells, which are attracted towards chemokines produced in the tumour. It is the T cells that ultimately damage the tumour cells [14]. The local inflammation, vessel dilation, and platelet aggregation take place after endothelial cells (ECs) destruction [14]. The main reasons for these events are the infiltration caused by the immune cells, production of thromboxane (TBX), cytokine-like interleukin 1β (IL1β), IL6, and IL8, also tumour necrosis factor-α (TNFα).

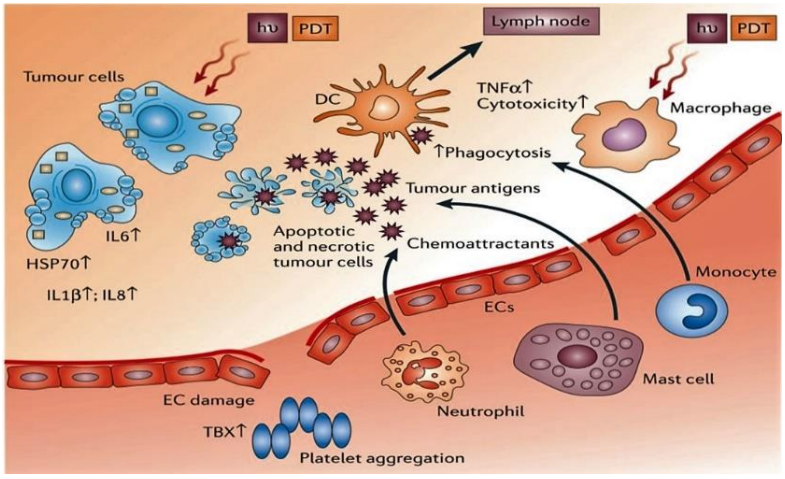

Figure 2.1:Illustration of tumour cells response in PDT. The initiation of the necrotic and apoptotic process due to $^1O_2$ generated in PDT kills the cancer cells. The figure is taken from [14].

2.2 Photodynamic therapy (PDT)

2.2.1 PDT working principle

Figure 2.2a shows the schematic representation of the photodynamic process. The first stage in treating the tumours present inside the body using PDT mechanism is the intravenous injection of PS which then infiltrates the tumour [11, 13]. Then after the accumulation of PS in tumour tissues, the

light of appropriate wavelength and energy is illuminated. The PS molecules absorb this light and become excited from the ground state (PS) to produce short-lived singlet excited state ($^1PS^*$). Some excited singlet state electrons release energy and produce fluorescence, which can be used for tumour imaging [8]. This excitation process follows the intersystem crossing where the excited electrons change spins and form long-lived triplet state ($^3PS^*$) [15]. The singlet state acts as the predecessor of the triplet state. The triplet excited state then follows the various reaction processes as shown in figure 2.2b. The primary and secondary photochemical reactions play a major role in the formation of free radicals which contribute to cytotoxicity (damage of the cancer cells). In the primary photochemical reaction, mainly due to photosensitizer sensitization, type I and type II reaction processes take place. In type I reaction, anion or cation is formed by transfer of a proton or electron, respectively.

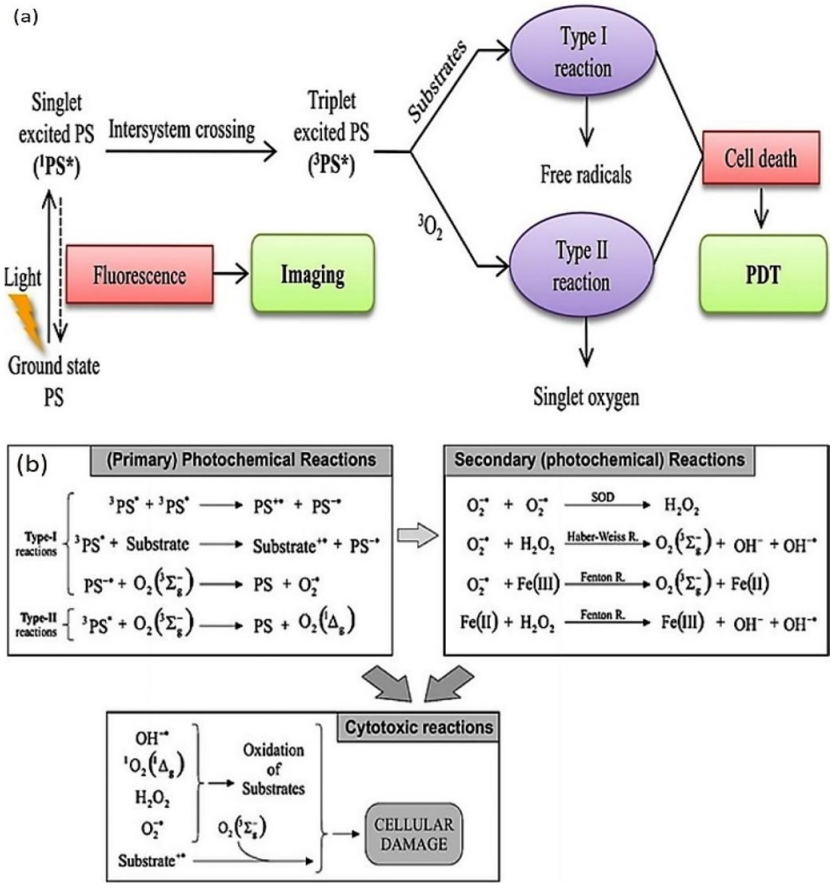

Figure 2.2(a) Schematic representation of photodynamic reaction. The figure is taken from [8]. (b) Shows the photochemical reactions occur during PDT. The figure is taken from [16].

This anion and cation then react with oxygen to form superoxide, hydroxyl ions, hydrogen peroxides. In type II reaction, the PS molecule from triplet state comes down to the ground state by emitting energy. In the secondary reaction, due to the reaction between oxygen, hydrogen peroxide, Fe (III) molecules small amounts of hydroxyl, and oxygen radicals are produced. Finally, these energy emissions activate the triplet ground oxygen to form singlet oxygen ($^1O_2$). The PDT efficiency mainly

depends on the PS chemistry, the chemical composition, PS localization in tumour cells, light energy and irradiation time, and the presence of molecular oxygen [17].

2.2.2 Photosensitizers

Many chemical compounds can generate $^1O_2$ (type I) and radicals (type II) on light irradiation, but only a few are practically applicable and clinically approved. The very first clinically approved photosensitizer is Photofrin [18-19], it is a hematoporphyrin derivative and approved in several countries including Canada, Japan, Europe, United States [20]. Table 2.1 shows the clinically approved photosensitizers that are approved by countries and are used in cancer treatment.

First generation photosensitizers

The first-generation photosensitizers such as Photofrin and similar hematoporphyrin derivatives are a mixture of monomers, dimers, and oligomers. These PSs have a distinct disadvantage. First, the light absorption intensity of these PSs is very low in NIR region which restricts the treatment of tumours present deep in the body. Therefore, only skin related cancers can be treated using these PSs. Second, the accumulation of drugs in healthy tissue even after tumour treatment causes photosensitivity in the patients for several weeks. The patient should remain in the dark for few weeks until the drugs degrade and are eliminated from the body. The advantage is that they have very high singlet oxygen quantum yields which ensure a considerable amount of $^1O_2$ generation upon light irradiation. Figure 2.3 shows the structures of Porphyrin-based photosensitizers.

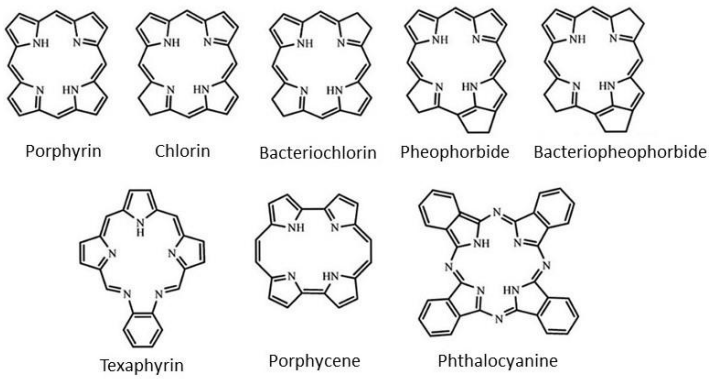

Figure 2.3: Porphyrin-based photosensitizers. The Figure is taken from [21].

Table 2.1: Show the clinically approved photosensitizers, their absorption peak wavelength λ_{max}, extinction coefficient (ε_{max}), and application. The table is taken from [21].

Compound	**Trademark**	**λ_{max} (nm) ε_{max} (M^{-1} cm^{-1})**	**SOQY**	**Clinical Application**
Porfimer sodium	Photofrin	(632) (3000)	0.89	Canada (1993)-bladder cancer; USA (1995)-esophogeal cancer; USA (1998)-lung cancer; USA (2003)-Barrett's sophagus; Japan-cervical cancer; Europe, Canada, Japan, USA, UK-endobroncheal cancer.
5-Aminolevulinic acid (ALA)	Levulan	632 (5000)	0.56	USA (1999)-actinic keratosis.
Methyl aminolevulinate (MAL)	Metvixia	-	-	USA (2004)-actinic keratosis.
Hexaminolevulinate (HAL)	Cysview	-	-	USA (2010)-bladder cancer diagnosis.
Benzoporphyrin derivative monoacid ring A (BPD-MA)	Visudine	689	0.84	USA (1999)-age-related macular degeneration.
Meta-tetra(hydroxyphenyl)chlorin (*m*-THPC)	Foscan	652 (35000)	0.87	Europe-neck and head cancer.
Tin ethyl etiopurpurin	Purlytin	664 (30000)	-	Clinical trials-breast adenocarcinoma, basal cell carcinoma, Kaposi's sarcoma, age-related macular degeneration.
N-aspartyl chlorin e6 (NPe6)	Laserphyrin, Litx	664 (40000)	0.77	Japan (2003)-lung cancer.
2-(1-Hexyloxyethyl)-2-devinyl pyropheophorbide (HPPH)	Photochlor	665 (47000)	-	Clinical trials-esophageal cancer, basal cell carcinoma, lung cancer, Barrett's esophagus.
Palladium bacteriopheophorbide (WST09)	Tookad	763 (88000)	0.50	Clinical trials-prostate cancer.
WST11	Stakel	-	-	Clinical trials-prostate cancer.
Motexafin lutetium (Lu-Tex)	Lutrin, Optrin, Antrin	732 (42000)	-	Clinical trials-prostate cancer, age-related macular

				degeneration, breast cancer, cervical cancer, arterial disease.
Aluminum phthalocyanine tetrasulfonate (AlPcS4)	Photosens	676 (200000)	0.38	Russia (2001)-stomach, skin, lips, oral cavity, tongue, breast cancer.
Silicon phthalocyanine (Pc4)	-	675 (200000)	-	Clinical trials-actinic keratosis, Bowen's disease, skin cancer, mycosis fungoid.

Second generation photosensitizers

The disadvantages of first generation photosensitizers such as low tumour selectivity, accumulation in healthy cells, low light absorption in NIR region encouraged researchers to formulate second generation photosensitizers. These second-generation photosensitizers are comprising of porphyrin and non-porphyrin compounds. Secondary porphyrin structures are chlorins, bacteriochlorins, phthalocyanines, pheophorbide becteriopheochlorins, texaphyrins [8]. Also, some nonporphyritic second generation PSs are anthraquinones, phenothiazines, xanthenes, cyanines, and curcuminoids [8]. Examples of such second-generation photosensitizers are shown in figure 2.4. These photosensitizers have light absorption and excitation wavelength in the NIR region i.e. above 630 nm and have high extinction coefficient. Second-generation photosensitizers have high SOQY. Their low cell accumulation allows faster degradation of PSs and faster treatment time.

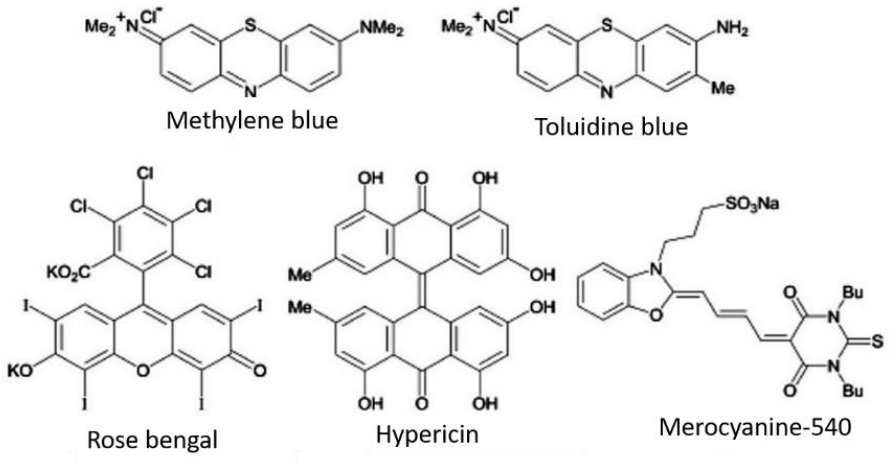

Figure 2.4: Shows the non-porphyrin based second generation photosensitizers. The Figure is taken from [21].

Third generation photosensitizers

Second generation PSs show some advantages over first generation PSs such as photosensitization in the NIR region, high extinction coefficient, deep tissue penetration, and low tissue accumulation.

However, in an aqueous medium, they lose the $^1O_2$ generation efficiency and hence tumour damaging efficiency as well as they lack cancer cells selectivity [8]. To overcome these shortcomings, PSs are being conjugated with tumour-specific peptides/ antibodies-/ or encapsulated in materials that can deliver PSs to the tumour cells [8]. Such PSs conjugated with delivery vehicles are called as third generation PSs.

Rose Bengal

The first mention of Rose Bengal appeared in the records of chemical manufacturer company CIBA-Geigy, which was synthesized by Richard Gnemb in 1881 [22]. It has many applications as in food industry, cosmetics, and wool dye. However, now it has been widely researched and used as a disease curing drug. After the research work of Oskar Raab on photodynamic therapy [23], followed by the work of Tappeiner and Jodlbauer on the use of a combination of dyes, light, oxygenation in photodynamic therapy [24]. Figure 2.5 shows the structure and UV-V light absorption spectrum of RB. Rose Bengal is a xanthene dye having green light absorption spectrum in the range of 480-550 nm. The RB has a negatively charged carboxylic group at the natural pH. The negatively charged carboxylic group (-COOH) is used for the covalent conjugation with the nanoparticles.

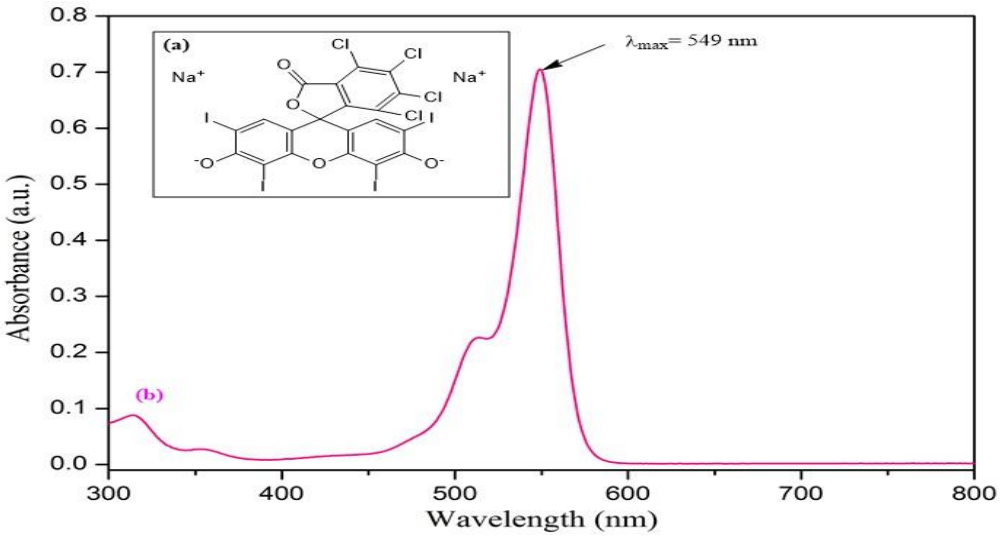

Figure 2.5: (a) Chemical structure of RB, (b) UV-Visible spectrum of RB in aqueous solution showing maximum peak intensity at 549 nm.

2.2.3 Light in PDT

The light of appropriate energy and wavelength is essential for the photosensitizer excitation and singlet oxygen generation. There are various kinds of light sources available in PDT. Lasers are beneficial in the treatment of tumours present inside the body as they can be easily coupled with optical fiber for direct tissue delivery. Many laser sources are available for use in PDT such Argon pumped dye lasers (wavelength range 488 and 514.5 nm), metal vapor lasers (in the ultraviolet or

visible wavelength range depending on the metal used), solid state lasers (wavelength range between 250 to 2000 nm) [25]. Femtosecond solid state lasers are useful in two-photon excitation of photosensitizers. In the two-photon excitation mechanism, two photons of the same wavelength are released from the source and then the combined energy of these two photons can be used to excite the photosensitizers, which require the excitation wavelength which is equivalent to the twice the wavelength of single photon [26]. Figure 2.6 shows the process of killing of the tumour. The photosensitizer is administered to the tumour tissue, and when the photosensitizer accumulates in the tumour tissue, it is activated by the laser source. The activated photosensitizer generates $^1O_2$ and damage cancer tissues. After the destruction of cancer cells, the body again regenerate the new normal tissues.

Apart from lasers, various lamps are also used in clinical treatment. Lamps are easy to maintain and available in wide range of wavelengths between 400-1100 nm. The light emitted by lamps cannot be coupled to fibers and thus is applicable for use in the treatment of cancers placed on the upper body surface. Other light sources are light emitting diodes (LEDs) and are widely used in laboratory experiments and clinical therapies. LEDs can emit monochromatic light in the range of ultraviolet (350 nm) to near infrared (1200 nm) [26]. LEDs are cheap and readily available.

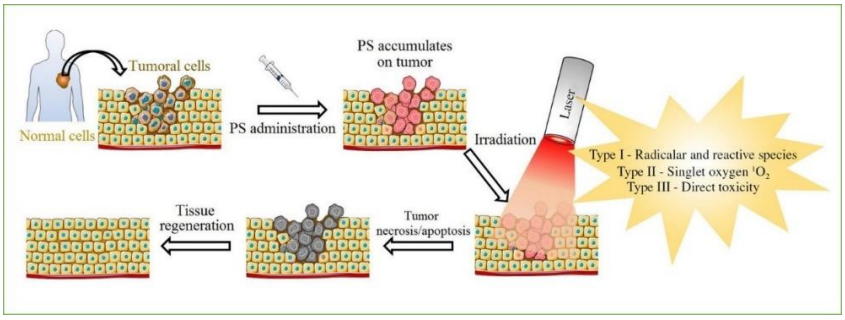

Figure 2.6: Shows the extinction of tumour by PS. The PS is administered in the tumour tissue, and then the laser light source is used to activate the PS which cause the death of tumour cells. The figure is taken from [27].

2.3 Nanoparticles in PDT

Limitations of photosensitizers such as unable to treat cancer placed deep in the body, less sensitive to near infrared (NIR) light, accumulation in the body after treatment and low $^1O_2$ generation efficiency minimize their applicability in cancer treatment. The use of photosensitizers in combination with nanoparticles can reduce these limitations and improve the photodynamic activity. The photodynamic efficacy of photosensitizers can be increased by conjugating them to nanoparticles by various conjugation methods such as covalent conjugation, electrostatic conjugation, encapsulation of photosensitizers to nanoparticles surface. Also, one or more photosensitizers along with cells specific ligands can be functionalized on the nanoparticles surface. Such multipurpose

nanodrugs improve tumour selectivity and photodynamic activity of photosensitizers. They must have following properties in order for nanoparticles to become applicable in PDT.

1. The nanoparticles should have a high surface to volume ratio to increase the photosensitizer loading capacity [28].
2. The nanoparticles surface must be easily functionalized with target specific groups for better cell targeting [29].
3. Nanoparticles can be encapsulated in the shell to convert hydrophobic materials to hydrophilic materials and vice versa for faster delivery.
4. Nanoparticles can be decorated with various drugs, target-specific ligands, and proteins, imaging agents to make them multifunctional [30].

Nanoparticles that are used in PDT are biocompatible nanoparticles, quantum dots, metal nanoparticles, upconversion nanoparticles. They are discussed in the following sections.

2.3.1 Biocompatible nanoparticles

Biocompatible nanoparticles are synthetic polymer-based nanoparticles. They are used as a drug delivery vehicle in PDT. They can enclose and carry a significant amount of photosensitizer drug and degrade quickly, therefore limiting the accumulation of nanoparticles in the body. The biocompatible nanoparticles when used as a carrier for photosensitizer drugs, improve the solubility of photosensitizers in tissues and eventually enhance the pharmacokinetics properties of photosensitizers. Also, after degradation, they do not produce any toxic elements that are harmful to the body and excreted out from the body via the natural physiological process. Some of the biocompatible nanoparticles used in PDT are described in this section. Dendrimers are macromolecules having branches like tree structure [31]. They are easily functionalized and modified for the application in PDT. Figure 2.7 shows various methods of attaching photosensitizer drugs to the dendrimer in PDT.

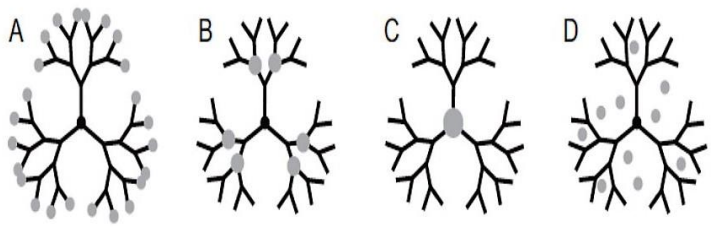

Figure 2.7: Shows the various methods to deliver drugs using dendrimer: (A) covalent attachment of drugs to dendrimers; (B) attaching drugs inside the dendrimer branches; (C) drugs as a core material; (D) encapsulating drugs inside dendrimer. The Figure is taken from [32].

The 5-Aminoevulinic acid (5-ALA), a clinically approved PSs and can be used to produce Protoporphyrin IX (PpIX) in cells and can be employed for the detection of tumour cells in PDT [33]. The porphyrin photosensitizer as a core and the dendrimer as the shell is as shown in figure 2.8 a, b. In this approach the dendrimer-porphyrin complex conjugate is targeted to the specific tumour location and light is irradiated on conjugate to generate $^1O_2$. The amount of $^1O_2$ produced was very low but still this amount is sufficient to damage the tumour cells [34].

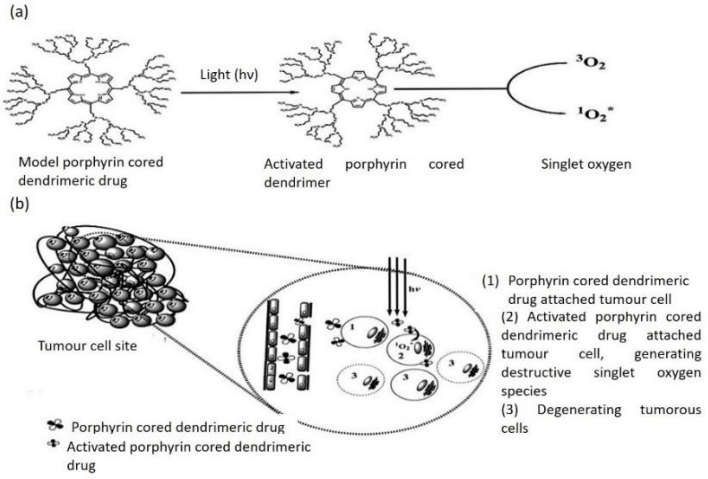

Figure 2.8: (a) Illustrate the porphyrin cored dendrimer activation and singlet oxygen generation; (b) Shows the effect of porphyrin cored dendrimer on the tumour cell. The figure is taken from [34].

Liposomes are another kind of biodegradable photosensitizer carrier. Liposomes are the spherical vesicles with one or more lipid bilayers that have a central aqueous core which stores drugs. Figure 2.9 shows the liposome with drug captured in the aqueous phase and inside the bilayer [35]. A verteporfin liposomal derivative Visudyne was approved for treating age-related macular degeneration in 2000 and pathological myopia in 2001 [36]. Liposomes are prepared from lipids such as phosphatidyl inositol, phosphatidyl serine, phosphatidyl choline. Moreover, it can be combined with other surface modifying agents to change the properties such as size, drug carrying capability [37]. Both hydrophilic and hydrophobic types of liposomes can be prepared depending on the nature of the drug, allowing delivery of any drugs to the tumour location [38]. Some photosensitizers aggregate in the water solution and lose their fluorescent efficacy so liposome conjugation with photosensitizers can improve fluorescence efficiency [39]. Liposomes with polyethylene glycol (PEG) coating were used to counter the aggregation of tetrakis (4-hydroxyphenyl) porphyrin (p-THPP) in the treatment of the prostate adenocarcinoma (DU 145) and human adenocarcinoma cell line (HCT 116) [40].

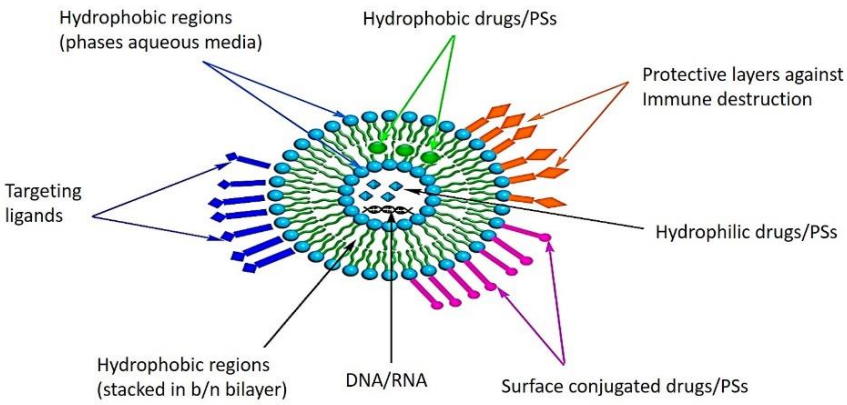

Figure 2.9: Illustrates the liposome structure in which drug entrapped in the aqueous phase and inside the bilayer. The figure is taken from [35].

In another study, silica (SiO_2) nanoparticles were conjugated with the RB PS molecules. The SiO_2-RB drug were used to kill the gram-positive bacteria together with Methicillin-resistant Staphylococcus aureus (MRSA) by using PDT [41]. The 9,10-anthracenedipropionic acid (ADPA) was used to detect the $^1O_2$ generated by the drug and the SOQY was 0.6 [41]. The reported quantum yield in this paper is lower than the RB (0.76) [4]. In the case of biocompatibility issue of SiO_2 nanoparticles, there is a need of more investigation. However, the toxicity of SiO_2 depends on the size, shape, surface chemistry and charge on particle [42].

2.3.2 Non-biodegradable nanoparticles

Non-degradable nanoparticles or inorganic nanoparticles contain a solid-state core covered with an organic shell enabling surface functionalization for tumour cell-specific ligands [43]. These nanomaterials have great potential to be used as a carrier in PDT due to the small size and high surface area to volume ratio, easy synthesis process, different surface functionalization techniques with target specific proteins and ligands. They can be synthesized from various materials, such as quantum dots (semiconductor nanoparticles), magnetic nanoparticles (oxides), or pure metal [44-47]. The photosensitizer drugs can be attached to the inorganic nanoparticles by covalent or electrostatic conjugation methods by modifying the surface of drugs and nanoparticles.

Quantum dots (QDs)

The QDs are spherical semiconducting nanoparticles having a size in the range of 1 to 10 nm. Due to their small size and fluorescent properties, they can transfer energy to the photosensitizers through fluorescence resonance energy transfer (FRET). In the FRET mechanism, the QDs in excited state transfer energy to the photosensitizer through the dipole-dipole coupling or they can react directly with molecular oxygen through energy transfer mechanism to generate $^1O_2$ in PDT [48]. QDs can be synthesized to match the properties of photosensitizer [49]. The silicon phthalocyanine photosensitizer was conjugated to CdSe QDs through an alkyl linkage. Through FRET mechanism

the CdSe QDs activated the emission of silicon phthalocyanine at 680 nm and generated the $^1O_2$ for PDT in cancer treatment [49]. In this process, the functionalized QDs also generated $^1O_2$ regardless the photosensitizers [49]. Figure 2.10a shows the structure of QD and figure 2.10b illustrates the generation of $^1O_2$ from QD photosensitizer drug composite.

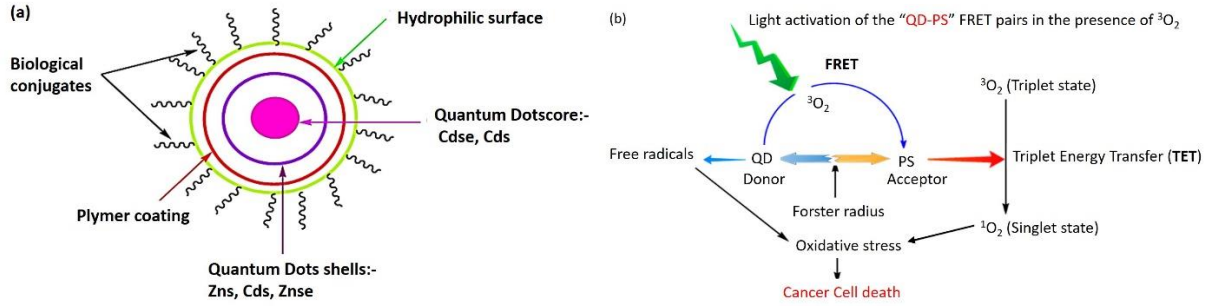

Figure 2.10: (a) Shows the schematic of QD as core and polymer coating functionalized with biological conjugates. (b) Illustrates the destruction of cancer cells due to generated $^1O_2$ when light falls on QD-PS conjugate. The QD also produces $^1O_2$ in a tiny amount on light irradiation. The figures are taken from [50].

In another approach, the QD were coated with the phytochelatinrelated peptides and then the RB (QD-RB) and chlorin e6 (QD-chlorin e6) PSs were covalently conjugated to the surface of peptides [51]. The CDse/CdS/ZnS nanocrsystals were as a core nanocrystals and photosensitizer-peptide conjugates were used as coating. Anthracene propionic acid (APA) was used for chemical detection of $^1O_2$ and the conjugates, QD-RB and QD-chlorin e6 were excited by using Nd:YAG laser of 532 and 355 nm, respectively. The maximum SOQY for QD-RB was 0.17 and for QD-chlorin e6 was 0.31 [51]. The reduction in quantum yield might be due to the direct photosensitizer excitation, quenching in PSs due to conjugation between QD and PSs.

Metal nanoparticles

When light falls on the metal nanoparticle, its electrons undergo localized surface plasmon resonance (LSPR). Due to the property of SPR and capacity to produce heat on light absorption Gold nanoparticles are widely used in PDT and photothermal therapy (PTT) [52]. The plasmon resonance property of metal nanoparticles also helps to improve the $^1O_2$ generation of PSs in PDT [53-54]. Metal nanoparticle conjugation with PSs helps the PSs to absorb more light and thus increase the $^1O_2$ generation efficacy [53-54]. The aqueous solution of nanoparticles of silver (Ag), gold (Au), and platinum (Pt), when excited with the light in the region of their SPR bands generates $^1O_2$ [55].

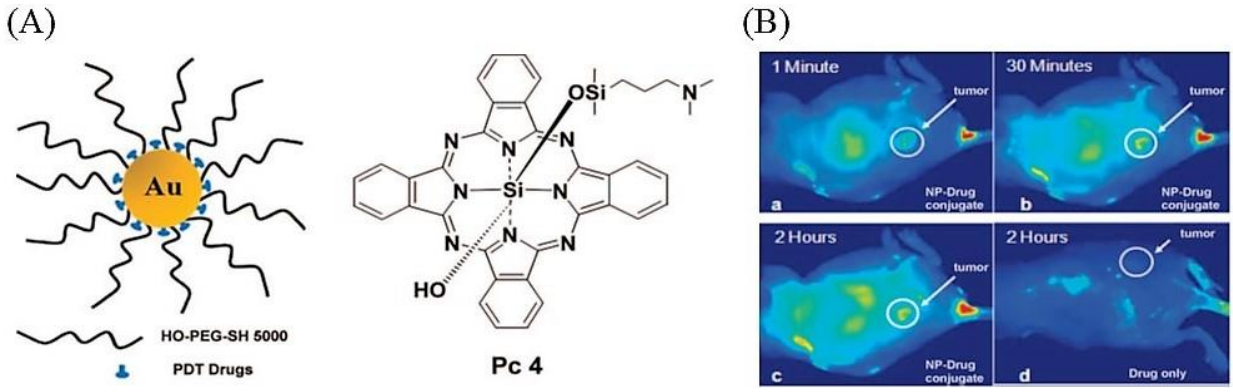

Figure 2.11: (A) Schematic representation of AuNPs conjugated Pc 4 photosensitizer and Pc 4 drug structure. (B) Fluorescence Figures of mouse model having tumour injected intravenously with Au-Pc 4 drug (a) 1 min, (b) 30 minutes, (c) 2 hours shows the bright spot due to the presence of Pc 4 in tumour region. (d) A mouse injected with only Pc 4 drug without AuNPs conjugation showing no drug circulation without AuNPs conjugation after 2 hours. The figure is taken from [56].

The gold nanoparticles with polyethylene glycol (PEG) were conjugated to the hydrophobic Pc 4 drug and tested in vivo in mice model bearing cancer tumour as shown in figure 2.11 [56]. They stated that the drug delivery time of Au-Pc 4 conjugates were less than 120 minutes whereas for no conjugated drug took 2 days to reach the cancer site [56]. The $^1O_2$ generated by the Au-Pc 4 conjugation was same as the $^1O_2$ generated without AuNPs conjugated Pc 4 photosensitizer [56].

Methylene blue (MB) photosensitizer was conjugated with polystyrene-alt-maleic acid coated AuNPs (Au@polymer / MB NP) has shown better SOQY (50 % more) compared to free MB molecules colliding light irradiation at 660 nm wavelength [57]. A further conjugation of Au@polymer / MB NP with transferrin, to ensure the selectivity to HeLa cells, doubled the efficacy of PDT on HeLa cells compared to free MB molecules at the same MB dose [57]. In another study, surface enhanced Raman scattering (SERS) active gold nanochains (Au-HA-HCA_n) were prepared by conjugating citrate stabilized gold nanoparticles with hyaluronic acid (HA) and hydrocaffeic acid (HCA) [58]. Then these gold nanochains (Au-HA-HCA_n) were conjugated with pheophorbide a photosensitizer (pheo a), and the cellular uptake of this drug in HeLa cells was examined [58]. The above examples prove that the gold nanoparticles surface is easily modified with semiconductor or polymer coating and can be functionalized with drug or cell targeting ligands to increase the efficiency of photodynamic effect of drugs. Also, due to the small size and good clearance from the body indicates they are biocompatible. All these properties of gold nanoparticles make them potentially useful in PDT.

Upconversion nanoparticles

Conventional PDT derivatives are widely used because of their low dark toxicity and cell selectivity [59-60]. However, the photosensitizer in conventional PDT requires high energy light (UV or visible light) to activate which cause damage to normal cells and cannot be used to treat deep tissue cancers

[61]. Deep tissue penetration can be achieved by using low energy near infrared light (NIR) without damaging normal cells [62]. The synthesis of NIR light activated photosensitizer is hard. However, upconversion nanomaterials can be used to achieve the use of NIR in PDT. Upconversion nanoparticles absorb low energy source light (NIR) and emit high energy light (UV or visible). The upconversion nanomaterials are extensively applied in bioimaging and various cancer treatment. [62-64]. In upconversion nanomaterials, $NaYF_4$ as a host material in combination with the rare-earth materials such as lanthanides (La^{3+}) is most commonly used for converting NIR to UV or visible light [64]. For the better absorption NIR light, the lanthanides (La^{3+}) in host materials, Yb^{3+} are doped with the other materials ion such as Er^{3+}, Ho^{3+}, Tm^{3+} [64].

The figure 2.12a shows the $^1O_2$ generation mechanism in PDT when the NIR light falls on Yb^{3+} and Er^{3+} doped $NaYF_4$ UCNPs functionalized with ZnPc photosensitizer [65]. The figure 2.12b shows the various methods to synthesize the upconversion nanoparticles. In most cases, silicon dioxide is used for coating of upconversion nanoparticles as shown in figure 2.10b. The mesoporous silica coating is also used to attach the photosensitizer molecules on upconversion nanoparticles

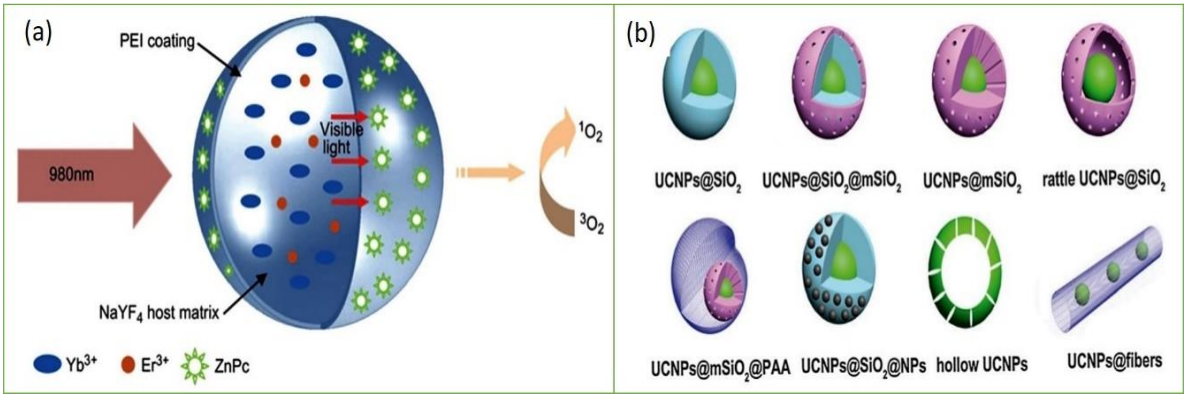

Figure 2.12: (a) Illustrates the working principle of UCNPs based PDT: UCNPs, when irradiated with 980 nm NIR light, converts the NIR light to visible light and excite the ZnPc photosensitizers to transform molecular oxygen into $^1O_2$. The Figure is taken from [65]. (b) Shows the upconversion nanoparticles (UCNPs) based drug carries. ($mSiO_2$: mesoporous silica, PAA: Poly acrylic acid, NPs: various nanoparticles like Au, Ag, Fe_3O_4). The Figure is taken from [66].

surface. The various method to synthesize and functionalization of upconversion nanoparticles surface include (i) sol-gel method [67], (ii) hydrothermal-assisted template method [68-69], (iii) self-assembly or polymer grafting [70], and (iv) electrospinning method [71].

Figure 2.13 shows the synthesis, mechanism of acting and in vivo PDT application of upconversion nanoparticles [72]. Here they co-doped the host $NaYF_4$ upconversion nanoparticle with Yb^{3+} and Er^{3+} ions to convert the NIR light of 980 nm into two similar high energy visible lights [72].

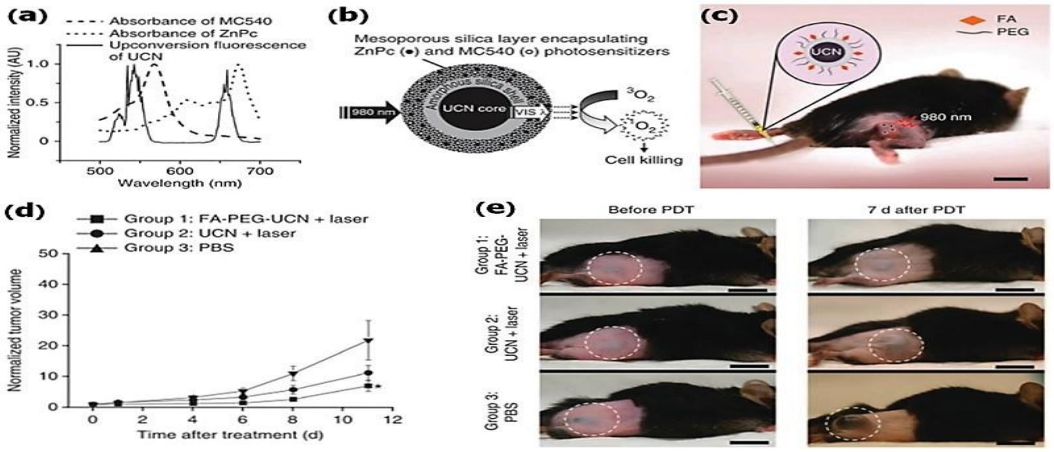

Figure 2.13: In vivo PDT treatment of melanoma tumour using upconversion nanoparticles. (a) the fluorescence emission and absorption spectra of upconversion nanoparticles (at 980 nm excitation) and ZnPc/MC540 photosensitizers, respectively. (b) Schematic representation of upconversion nanoparticles with mesoporous silica coating and ZnPc/MC540 functionalization. (c) Intravenous injection of upconversion nanoparticles in a mouse (FA-PEG-UCNPs). (d) Tumour volume changes after using various treatments. (e) The photos show the tumour volume change after injecting with FA-PEG-UCNPs, only upconversion nanoparticles, and PBS before and after PDT. The figure is taken from [71].

The two photosensitizers zinc phthalocyanine (ZnPC) and merocyanine 540 (MC540) were encapsulated in mesoporous silica. The use of two photosensitizers made it possible to achieve improved visible light absorption and increase the $^1O_2$ generation in PDT [72]. Also for the in vivo study, they attached folic acid (FA) with the ZnPc, MC540 conjugated upconversion nanoparticles to treat melanoma tumours in mice [72]. Their results showed that the upconversion nanoparticles in PDT activated by NIR light are advantageous than the conventional PDT treatments for deep-seated tumours.

3 Instrumentation and analysis methods for nanomaterials characterization

For the precise investigation of chemical and physical properties of any material, the characterization methods play a crucial role. The better understanding and proper use of the characterization instruments, materials properties, and analytical methods, help not only to minimize the errors but also to apply accurate measurement techniques. This chapter will give detail introduction of the theory and background of the characterization instruments used in the project. The dynamic light scattering measurement technique used to determine the size and the surface charge potential of NPs. The NPs` optical properties were investigated by using UV-Visible absorption spectroscopy and fluorescence spectroscopy. The main objective of this project is to quantify the $^1O_2$ generated by the RB, Au, and AuRB complex conjugate. We have used the indirect method of $^1O_2$ detection using SOSG probe method, which is discussed in detail in this chapter.

3.1 Nanoparticle characterization methods

3.1.1 Fluorescence spectroscopy

Fluorescence in photosensitisers

Whenever light falls on a substance molecule, it experiences absorption and/or scattering depending on the properties of the molecule. The substance molecule shows excitation after absorbing light, and the absorbed light is generally in the ultraviolet or visible range. Such substance is called a chromophore. So these chromophores molecules after absorbing a quantum of light get excited to the higher excited energy state. The molecules in the excited state degenerate energy very soon on a

ps time scale and falls to lower excited singlet state (within ns) and emit high energy light (nonradiative) or undergo transition producing heat (nonradiative). This excited state deactivation by releasing energy is known as fluorescence [73]. The wavelength range of the emission is higher than excitation wavelength range. The fluorescence also occurs by forbidden intersystem crossing (ISC) having a longer lifetime (10^{-5} to 10^{-8} seconds).

In photosensitizers, the macromolecules with double bond systems (π) show longer lifetime in the triplet state. The longer triplet state lifetime can generate more $^1O_2$. of The energy from triplet state can be released in two ways either by Type I mechanism or Type II mechanism. In Type I mechanism, the molecules transfer electron or proton to other atoms and generate superoxide while in Type II mechanism energy is delivered to the molecular oxygen [73]. This molecular oxygen on energy absorption converts to highly reactive $^1O_2$ from triplet oxygen state [73]. The Type II mechanism is preferable in PDT than Type II. The energy emitted from the excited singlet state of photosensitizers is used in fluorescence measurements.

Fluorescence intensity spectra

In the fluorescence property inspection of photosensitizers, two spectra are evaluated; one is the fluorescence excitation and the other fluorescence emission as shown in figure 3.1. The excitation spectrum is determined when the excitation wavelength is varied with emission keeping constant at a particular wavelength. When the photosensitizers molecules are well dispersed in solvents the absorption and excitation spectra, have the same shape. Figure 3.2 shows the excitation and emission spectrum. When the excitation is constant at one wavelength and emission is varied wavelength range, the fluorescence emission spectrum is obtained. The Stoke's shift is the variance between the emission and excitation maximum values.

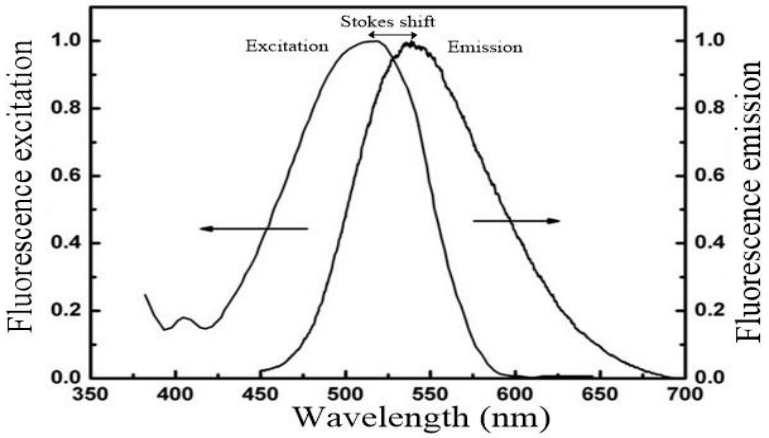

Figure 3.1: Excitation and emission spectrums. The figure is taken from [74].

Fluorescence lifetime and quantum yields

The fluorescence lifetime of the fluorophore is the average time spent by the molecule in its excited state before reaching to the ground state. The lifetime (τ) of the fluorophore is given by

$$\tau = \frac{1}{\Gamma + k_{nr}} \qquad 3.1$$

Where Γ and k_{nr} are emission rates and non-radiative decay rates, respectively.

In the case of radiative emission, the k_{nr} is zero and is called natural lifetime (τ_n) therefore the lifetime of the fluorophore is given as follows,

$$\tau_n = \frac{1}{\Gamma} \qquad 3.2$$

τ_n can be derived from the absorption spectra, extinction coefficient, emission spectra of the molecule.

The quantum yield of the fluorescence is calculated from the ratio of a number of photons emitted to the number of photons absorbed [75]. The rate with which fluorophore decay that is fluorescence quantum yield is given by

$$Q = \frac{\Gamma}{\Gamma + k_{nr}} \qquad 3.3$$

If the emission is non-radiative or less than the radiative decay, then the quantum yield is close to unity that is $k_{nr} < \Gamma$. The Stokes losses are the reason for the quantum yield value to be less than unity of the fluorescent materials [75].

Fluorescence Spectrometer

The fluorescence spectrometer is used to measure the excitation and emission spectra of fluorescent nanomaterials. Figure 3.2 shows the schematic of a standard fluorescence spectrometer. The Xenon lamp works as a source of excitation light and the scanning grating used to obtain the monochromatic light wavelength. When this monochromatic light of appropriate energy falls on the photosensitive material, the fluorescence is produced. Then released fluorescence from the sample is acknowledged by the detector present at the final stage. The fluorescence data received by the detector is transferred to the computer software which analyzes and plots the fluorescence intensity (excitation or emission) versus wavelength graphs and displays.

All fluorescence measurements in this work were taken on a Cary Eclipse Fluorescence Spectrophotometer. For sample measurements, the excitation wavelength of 488nm was used to create the fluorescence in the solution in the range of 500-600 nm with the slit width of 5 nm. The

source voltage was kept in the medium range. The measurements can be performed in a glass or quartz cuvettes.

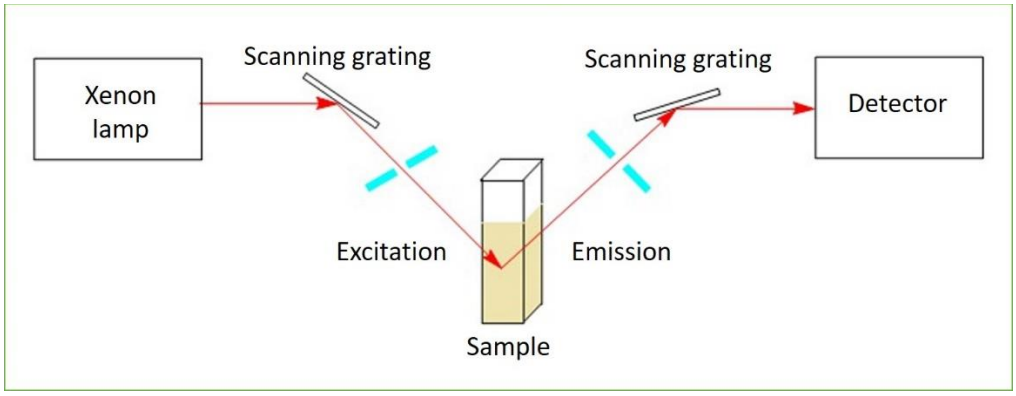

Figure 3.2: The generalize schematic of fluorescence spectrometer

3.1.2 UV-Visible Absorption Spectroscopy

For the light absorption studies of the nanomaterials, Carry 5000 UV-VIS-NIR spectrophotometer was used. Ultraviolet-visible spectroscopy (UV-Vis) or ultraviolet-visible spectroscopy refers to absorption or reflectance of light in the ultraviolet-visible light intensity range. The light absorbance and reflectance the color of chemicals are affected by the absorption or reflection of light in the visible spectrum. Due to absorption or reflection, the chemical molecules experience electronic transition. So this process is opposite compared to the fluorescence spectroscopy where the transition takes place from higher state to the lower state [76].

The UV-Vis spectrometer measures the light intensity passed through the sample (I) with the initial incident light intensity (I_0). The transmittance (T) is the ratio of diffused light from the sample and the incident light on the sample, i.e., I/I_0. The absorbance, A is defined as,

$$A = - \log (\% T / 100 \%) \quad 3.4$$

The spectrometer incorporates a light source, a sample holder, monochromators, and at a final stage detector. The light source can be a tungsten filament (300-2500nm), Xenon arc lamp (160-2000 nm) [76].

The detector is typically a photodiode, or a photomultiplier tube or photodiode array. For the use of light of only one wavelength, the monochromator is used along with the detectors. The monochromator rotates a diffraction grating to measure the intensity of light as a function of wavelength. Also, the monochromators fixed with the matrix of CCDs and photodiodes are used to receive and detect the light intensities at multiple wavelengths, simultaneously. There are two types of spectrometers, single-beam, and double-beam. In the single-beam spectrometer, first, the original intensity I_0 is measured without placing the sample and then measured with the sample. While in the double-beam spectrometer, the light coming through monochromator is divided into two by the beam

splitter. One light beam transmits through the reference sample and the other through the actual specimen. The intensity of the reference light beam is considered as the 100% Transmission intensity i.e. no absorbance. The result displayed is the ratio of reference intensity and specimen intensity.

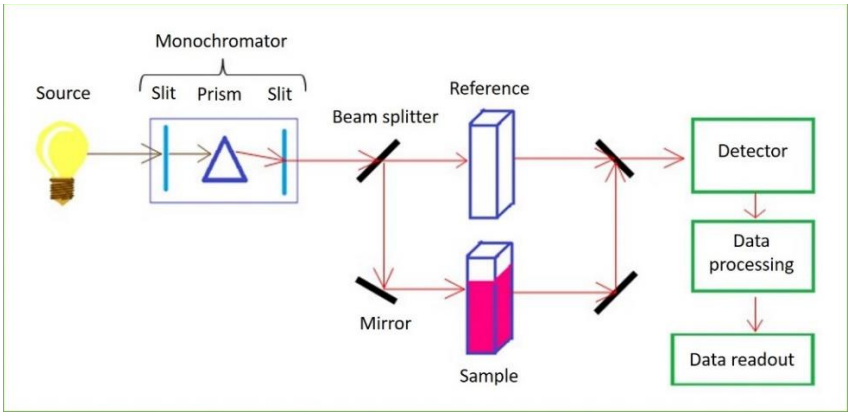

Figure 3.3: The figure shows generalized schematic of UV-VIS-NIR spectrophotometer

3.1.3 Size and surface potential measurement

The Zetasizer is composed of analyzers which can measure the particle size, surface zeta potential and molecular weight of the particles. It can analyze the particles or molecules ranging sizes from nanometers to micrometers. The instrument uses various light scattering techniques for the analyzing particles. The dynamic light scattering is used to measure particle size, electrophoretic light scattering to investigate particle surface potential, and static light scattering to measure the molecular weight of the particle. The Zetasizer Nano ZS from Malvern Instruments was used to measure colloidal stability (surface zeta potential) and the size of the nanoparticle.

Surface Zeta potential measurement

The surface zeta potential measurements is a methodology to investigate the particle colloidal stability. The colloidal stability depends on in the surface potential of a particle in solution. So it measures the surface charge of a particle in solution. The NPs surface can be either positively charged or negatively charged which attracts the opposite charge and form thin layer close to the surface. The opposite charged thin layer is strongly attached to the NPs surface and forms a layer called Stern layer. The thin layer is outside to Stern layer which the excess number of positive ions than negative ions balance the Stern layer. Figure 3.4 shows the negatively charged nanoparticle attracts the positive ions on its surface and forms different layers around its surface. The double layers of the Stern layer and the thin layer is useful to measure the forces between colloidal particles. The hypothetical boundary within the diffuse layer, inside which ions and particles are stable is called as slipping plane. The ions inside the slipping plane move with the particle while the ions outside this plane stay stable. The potential across this layer is the zeta potential. Particles having zeta potential above + or -30 are

considered as stable and do not agglomerate. The surface zeta potential of the particles can be calculated using the Henry's equation

$$U_E = 2\varepsilon z \frac{f(ka)}{3\eta} \qquad (3.2)$$

Where U_E is the electrophoretic mobility and is calculated by Laser Doppler Velocimetry, ε dielectric constant, η is the viscosity of the medium, z is the zeta potential, f(ka) is Henry's constant.

From the above equation, the velocity of these particles depends on various factors such as applied electric field, viscosity (η) of the solution, the dielectric constant value of the medium, and the surface charge of immersed particles in the medium.

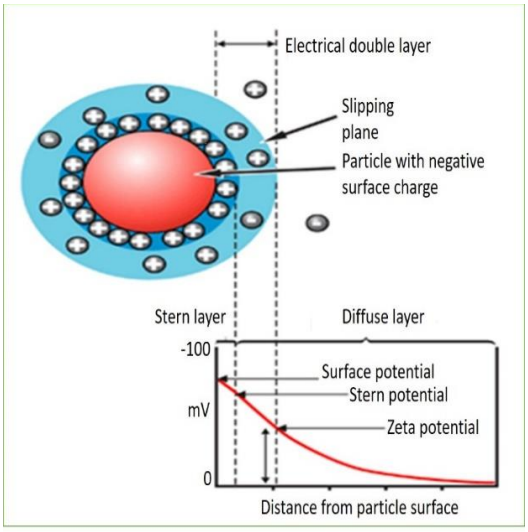

Figure 3.4: The diagram shows the potential distribution at the nanoparticle surface immersed in the solution. The figure is taken from [77].

Nanoparticles size measurement

All the nanoparticles in a liquid undergo Brownian motion. When light falls on the particles, the particles diffused and due to this, the intensity of light fluctuates. In dynamic light scattering (DLS), the rate of light intensity fluctuation and eventually the speed of particles diffusion is measured. The particles size measured by using the Stokes-Einstein's equation

$$d(H) = \frac{kT}{3\eta\pi D} \qquad (3.3)$$

In this equation, d(H) is a hydrodynamic diameter, k is Boltzmann constant, D is translational diffusion coefficient, T is absolute temperature, η is viscosity.

The particle diameter depends on the diffusion speed of the particle in the liquid medium it means that the measured size is the hydrodynamic diameter. The diameter measured using this technic has the same translational diffusion coefficient as the particle [77]. The translational diffusion coefficient depends on the ionic strength of the liquid medium and particles surface structure. This

instrument software uses the Mie light scattering theory to transform the light intensity distribution measurements into the volume [77]. Figure 3.5 shows the optical configuration of the Zetasizer Nano ZS. The particles size measurement dispersed in the fluid; the light is irradiated by the laser setup on the sample placed in the cell compartment. Then the light that falls on the particles is scattered in all directions. In the Zetasizer Nano ZS series instrument, the light scattered at the angle of 173° is collected to measure the particle size. So, the light scattered at 173° is received by the detector. The attenuator helps to limit the amount of light that is emitted from the laser source to avoid the saturation of the detector due to extra scattered light received it. The attenuator adjusts the intensity of light released from laser as per the change in the size of the nanoparticles. For tiny particles, it allows high-intensity light, and for large particles having the high scattering capacity, it allows low-intensity light. Then digital signal processor known as correlator receives the scattered light from the detector and calculate the change in scattered light intensity with respect to time. Finally, the computer software processes this information and measures the size of particles.

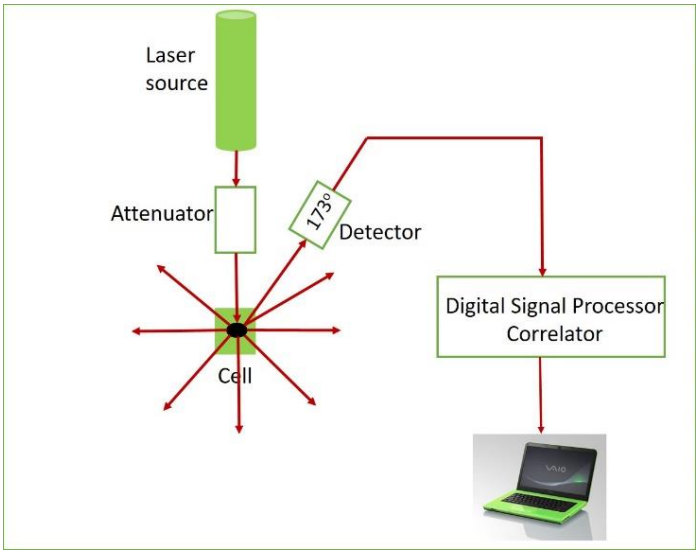

Figure 3.5: The figure shows the optical configuration of Zetasizer Nano ZS.

3.2 Singlet oxygen detection

In PDT, the $^1O_2$ is considered as the most significant cytotoxic agent. Along with the generation of $^1O_2$, its detection is the primary goal in PDT. The photosensitiser molecules on light absorption of the specific wavelength excite from the ground state to the unstable excited state. As in the excited state, the molecules are not stable; they return to the ground state by releasing some energy in the surrounding. The oxygen species present in the surrounding medium absorb this energy and produce the cytotoxic $^1O_2$ which kills cancer cells in PDT.

3.2.1 Singlet oxygen detection processes

The detection of $^1O_2$ generated by photobleaching of photosensitizer can be carried out by the direct method or indirect method. The direct method involves the detection of $^1O_2$ at its phosphorescence wavelength i.e. 1270 nm in steady state [78] or using time-resolved FTIR spectroscopy [79]. The detection of $^1O_2$ detection in HeLa cells using its 1270 nm luminescence and using 23 H-porphine (TMPyP), tris(2,2'-bipyridyl) dichlororuthenium(II) hexahydrate ($[Ru(bipy)_3]^{2+}$), hypericin, and pyropheophorbide-a (PPa) as photosensitizer materials were performed for steady state and time resolved spectroscopy [78]. The probability of successful detection of $^1O_2$ is very low with these techniques. The indirect detection methods include the $^1O_2$ detection using chemiluminescent sensor probes. The advantage of the sensor probes over direct detection methods in that they are very efficient in imaging $^1O_2$ detection in cells and the fluorescence produced can be easily sensed by the photosensitive detectors. In our project, we used the commercially available SOSG probe to sense the $^1O_2$ generated by RB and AuRB conjugates.

3.2.2 Singlet Oxygen Sensor Green (SOSG) reagent

The SOSG is a commercially available $^1O_2$ detection probe. It is commonly used as fluorescence detection probe in nanomaterial science, and biomedical application. The SOSG shows high affinity and sensitivity towards $^1O_2$ and is soluble in water [80]. The literature indicates the SOSG is made up of fluorescein (Fl) and anthracene (An) dye derivatives [81-82]. As shown in figure 3.6a in the SOSG probe, the anthracene donates an electron to the covalently conjugated electron acceptor Fl. The An highest occupied molecular orbital (HOMO) energy is greater than that of the Fl [83]. In the $^1O_2$ detection process, the An quenches the Fl in its excited singlet state by the photoinduced electron transfer [83-84]. This results in the reduction of an electron in Fl and Al cation formation [81]. On reacting with $^1O_2$, SOSG produces endoperoxides (EP). SOSG has very low reactivity to hydroxyl or superoxide ions like other detection probes [84]. In the absence of $^1O_2$, SOSG has blue fluorescence with emission maxima at 395 and 416 nm. The RB photosensitizer in aqueous solution when irradiated with the 532 nm green laser and fluorescence reading taken in the wavelength range 500 to 600 nm and at 488 nm excitation wavelength, shows green fluorescence with a maximum emission peak at around 525 nm. Figure 3.6 shows the SOSG fluorescence intensity of RB and the SOSG probe aqueous solution before and after irradiation of 532 nm laser.

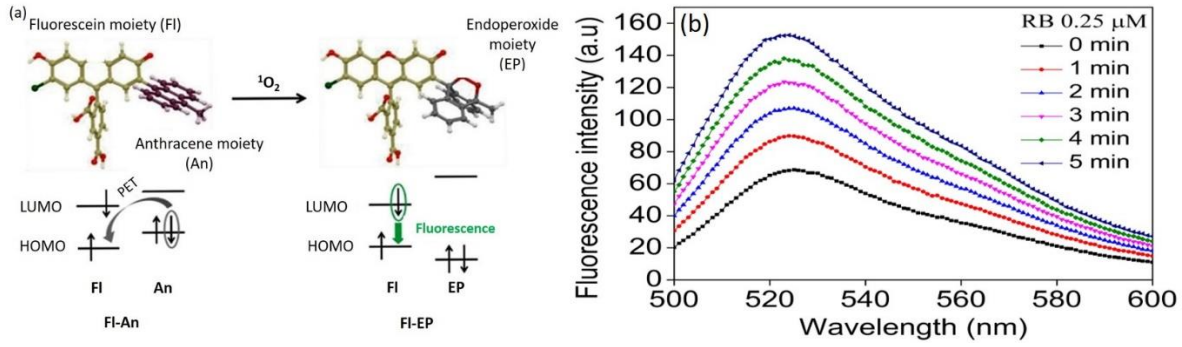

Figure 3.6:(a) Illustrates the structures of fluorescein (Fl) and anthracene (An) and proposed structure of SOSG on reaction with $^1O_2$. The figure is taken from [84] (b) Shows the SOSG fluorescence intensity of RB and SOSG probe in water, before and after irradiation of 532 nm laser.

Fluorescence dependency on pH

The pH of the photosensitizer material plays a major role in fluorescence spectrum. The addition of nanoparticles with different concentration (increasing or decreasing) may alter the pH of the aqueous solution. Moreover, this affects fluorescence reading of SOSG probe.To address this problem, we modified the fluorescence intensity of SOSG for the different pH values of nanoparticles. The SOSG probes fluorescence intensity dependency on pH is significant because of the pH value changes for the different concentration of nanoparticles. The SOSG probe was introduced into the aqueous solution of various pH. Here in this experiment, we inspected the shift in fluorescence intensity of SOSG probe with the pH. The pH value of the SOSG aqueous solution was varied by adding different concentrations of HCL and NaOH. Figure 3.7 shows the variation in SOSG intensity with the change in pH value.

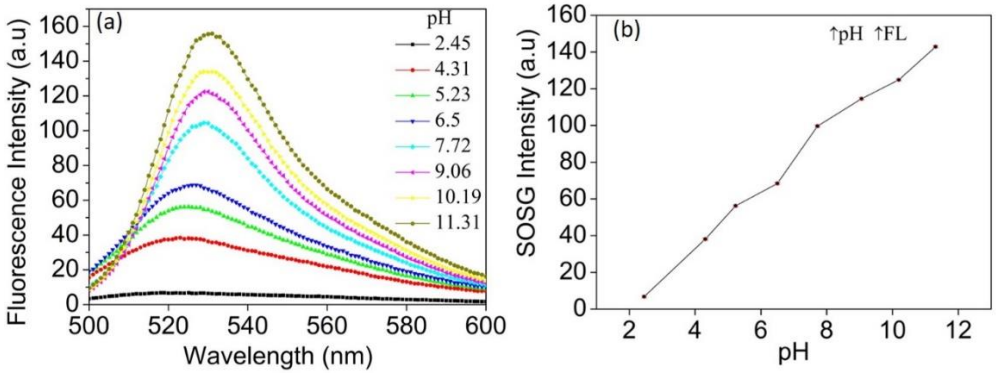

Figure 3.7: (a) Change in SOSG fluorescence intensity with pH value in DI water (b) SOSG intensity with the increase in pH value.

Statistical analysis

The output data were processed and plotted using Origin8.5 software (OriginLab Corporation, Northampton, MA, USA). The figures were designed using ChemDraw Professional 15.0 software (PerkinElmer, London, UK).

4 Experimental procedure, results and discussion

In this work, the idea is to improve the SOQY of the RB by conjugating it with the noble metal AuNPs. The AuNPs Surface Plasmon Resonance (SPR) properties may help in improving the $^1O_2$ generation capability of RB. Also, the toxicity effect of AuNPs has not taken into consideration in this project as there is a need of more investigation to study the toxicity of AuNPs. In this chapter, I have described the nanomaterials synthesis process and results of our experiments. The synthesis process, the AuNPs formation and then the covalent conjugation of Au with RB has been explained. Then I described $^1O_2$ generation efficiency with the various concentration of RB, Au-NPs, and AuRB complex conjugate. By repeating the photosensitization experiment with different concentrations of photosensitizers and photosensitizer nanomaterials complexes, I investigated the consistency and linearity of photosensitizer concentration to produce $^1O_2$. Finally, from the graphs of the rate of reaction versus absorption intensity of NPs conjugate, the SOQY of generated $^1O_2$ was calculated.

4.1 Experimental procedure

Materials

Sodium Citrate Dihydrate, Rose Bengal, methanol, Gold(III)chloride trihydrate, N-(3dimethylaminopropyl) N-ethylcarbodiimide (EDC) and 2-(N-Morpholino) ethanesulfonic acid (MES) buffer were purchased from Sigma-Aldrich, Australia and were used without further purification. Singlet Oxygen Sensor Green (SOSG) probe was purchased from Invitrogen, USA. The Rose Bengal (1mM) stock solution was prepared by dissolving 10.17 mg in 10 mL of water, and the prepared solution was stored in the dark to avoid photobleaching.

SOSG probe preparation

The SOSG (500 µM) stock solution was formed by adding 330 µL of methanol. I prepared two such SOSG vials and then mixed them together to use for further experiments. This solution was preserved at a 4° c temperature in a dark environment.

Synthesis of Au nanoparticles

Gold nanoparticles (AuNPs) were prepared by using a reduction method described in the literature [85]. Gold (III) chloride trihydrate used as a precursor for AuNPs and sodium citrate dihydrate as a reducing agent. In the complete experimental procedure, Millipore water was used. The 40mL of 1mM $HAuCl_4$ $3H_2O$ solution was heated to the boiling point while stirring with the magnetic bar. When the solution started boiling at about 95° C, 4mL of 38.8mM sodium citrate dihydrate solution was added. In the reduction process of gold(III) chloride trihydrate, first, the mixture became colorless then black and finally it turned deep red in color. The solution was kept to cool down at room temperature for 30 minutes in dark surrounding and stored at a 4° c temperature.

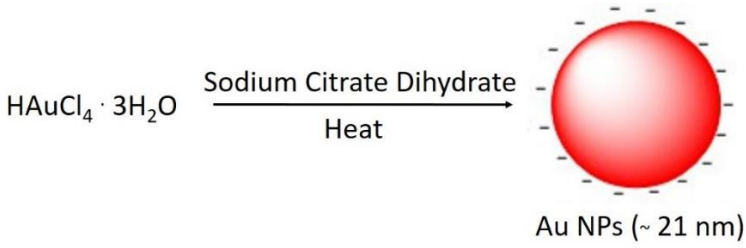

Figure 4.1: Show the schematic of Au nanoparticles synthesis process.

Preparation of AuRB complexes

To prepare the covalent conjugate, firstly, the NH_2 group was bound to as-prepared Au nanoparticles by adding 600 µL of 0.88 mM Thiol-PEG-NH_2 to the 10mL of Au and stirred for 3 hours. Secondly, 1.2 mL of the above mixture was taken, centrifuged and then mixed with 500 µL of the MES buffer. After that, to activate the carboxylic group of RB, 10 µL of RB from stock solution was added to 3 mL of MES buffer and 5 mg of EDC and allowed to react for 30 min. The MES buffer maintained the pH at 6.1. Here the appropriate amount of EDC and pH 6.1 ensured there is no nanoparticles aggregation due to electrostatic repulsive force loss during cross-linking and to maintain hydrolysis respectively. Then Au-PEG-NH_2 in MES buffer was added to the RB reaction medium and stirred for 3 hrs. Finally, the conjugate was purified by centrifugation for 20 min at 10,000 rpm, and mixed with 3 mL DI water. The similar procedure was followed to produce AuRB conjugates by adding 20 µL (conjugate M1), 30 µL (conjugate M2), 40 µL (conjugate M3) of RB.

4.2 $^1O_2$ detection, and measurement

Generation of $^1O_2$

To generate $^1O_2$, the conjugates were illuminated with a diode pumped solid state laser source at 532 nm wavelength. The incident laser driver current ratings set to 0.40 Ampere. The incident laser power density was 119 mW/cm^2. The laser illumination was from the top. For measurement purposes, the cuvette was filled with 2 mL of the conjugate sample and open from the top side. The total illumination time was 5 minutes.

$^1O_2$ detection using SOSG probe

The SOSG concentration was kept constant at 6 μM while the concentration of RB, Au-NPs was varied in the range 0.25-1.0 μM and 10-50 μM, respectively. The 488 nm excitation wavelength was used to measure the fluorescence spectra in the range of 500-600 nm keeping the spectral resolution of 5 nm. After every 1 minute of light irradiation, the cuvette containing sample was shaken well and placed in the fluorescence spectrometer for $^1O_2$ detection.

Determination of $^1O_2$ generation quantum yield

For the quantum yield measurement of singlet oxygen, I adapted the method described in the literature [86]. In this study, the rate of reaction (r) of SOSG with $^1O_2$ generation was calculated from the change in fluorescence spectrum with respect to time in a sample where concentration of RB is constant. The rate of reaction is directly proportional to the concentration of SOSG, as described by the following equations.

$$R_{PS} = \frac{\mathrm{d[SOSG-EP]}}{\mathrm{dt}} = k\,[SOSG]^n\,[^1O_2]_{PS} \qquad 4.1$$

$$R_{REF} = \frac{\mathrm{d[SOSG-EP]}}{\mathrm{dt}} = k\,[SOSG]^n\,[^1O_2]_{REF} \qquad 4.2$$

Where [SOSG-EP] is the SOSG-EP concentration; [SOSG] and [$^1O_2$] indicates the concentrations of SOSG and $^1O_2$ respectively; n is the order of reaction which depends on SOSG concentration. Here to maintain the rate of reaction proportional to the $^1O_2$, the order of the reaction (n=0) needs to be zero. The concentration of SOSG and photosensitizer are chosen to keep reaction order zero. The SOSG concentration was 6 μM in all the experiment and RB concentration was maintained maximum up to 1 μM [86].

In this project, during the $^1O_2$ generation experiment, the prepared photosensitizers (PS) and reference photosensitizers (REF) were sensitized by the same number of photons with the same wavelength, η_{phot}. The number of photons absorbed by PS and REF is denoted by η_{PS} and η_{REF}, respectively. Moreover, $\eta_{PS} = \eta_{phot}(1\text{-}T_{PS})$ and $\eta_{REF} = \eta_{phot}(1\text{-}T_{REF})$, T_{PS} and T_{REF} are transmittance

of PS and REF photosensitizers, respectively [87]. The value of the transmittance was calculated from UV-vis absorbance of the PS.

The SOQY of PS, φ_{PS} is the ratio of the number of $^1O_2$ molecules generated in unit volume to the number of photons absorbed by the PS, η_{PS}.

$$\varphi_{PS} = V\,[^1O_2]_{PS}/\eta_{PS}$$

Also for reference PS,

$$\varphi_{REF} = V\,[^1O_2]_{REF}/\eta_{REF}$$

From equation 4.1 and 4.2, we can get the following relation,

$$[^1O_2]_{PS} = \frac{R_{PS}}{R_{REF}}\,[^1O_2]_{REF}$$

Eventually, we get,

$$[^1O_2]_{PS} = \frac{R_{PS}}{R_{REF}}\,[^1O_2]_{REF} = \frac{R_{PS}}{R_{REF}}\,\varphi_{REF} * \frac{\eta_{REF}}{V}$$

This gives,

$$\varphi_{PS} = V\,[^1O_2]_{PS}/\eta_{PS} = \frac{V}{\eta_{PS}}\,\frac{R_{PS}}{R_{REF}}\,\varphi_{REF} * \frac{\eta_{REF}}{V} = \frac{R_{PS}}{R_{REF}}\,\varphi_{REF}\,\frac{(1-T_{REF})}{(1-T_{PS})}$$

Finally, the SOQY of PS is given by simplifying the above equation,

$$\varphi_{PS} = \varphi_{REF}\,\frac{R_{PS}/(1-T_{PS})}{R_{REF}/(1-T_{REF})} \qquad 4.4$$

$$\varphi_{PS} = \varphi_{REF}\,\frac{R_{PS}/\beta_{PS}}{R_{REF}/\beta_{REF}} \qquad 4.5$$

Where, $(1\text{-}T_{PS})$ and $(1\text{-}T_{REF})$ are β_{PS} and β_{REF} respectively. The equation 4.4 shows that the SOQY can be calculated from the known SOQY of reference photosensitizer. The above equation applies to the wavelengths where SOSG absorption is minimum (for us at 565 nm).

Further, for the measurement of $^1O_2$ generated from Au-NPs, AuRB conjugate and for convenience purpose, the equation 4.4 has been redefined in the following way,

$$\varphi_{Au} = \varphi_{RB}\,\frac{R_{Au}/\beta_{Au}}{R_{RB}/\beta_{RB}} \qquad 4.6$$

$$\varphi_{AuRB} = \varphi_{RB}\,\frac{R_{AuRB}/\beta_{AuRB}}{R_{RB}/\beta_{RB}} \qquad 4.7$$

Where φ_{Au}, φ_{AuRB}, φ_{RB} indicate the quantum yields of AuNPs, AuRB conjugate, and RB, respectively. φ_{RB} of the RB is 0.76 [4]. R_{Au}, R_{AuRB}, and R_{RB} indicate the rate of reaction of the SOSG probe with $^1O_2$ produced from the photosensitization of Au, AuRB, and RB, respectively.

4.3 Design of NPs-PS conjugates

In this work, the AuNPs were synthesized by reduction of gold (III) chloride trihydrate using sodium citrate dihydrate. The sodium citrate reduced gold precurser AuNPs. The AuNPs surface was functionalised by Thiol-PEG-NH_2 group. The carboxylic group (-COOH) on RB was activated using EDC. The surface modification of AuNPs and RB was carried out for conjugation purpose. In the covalent conjugation of Au and RB, the amine group of Au and -COOH of RB shares one electron and forms covalent bond. The covalent conjugation enables a strong attachment of RB molecules to the AuNPs surface.

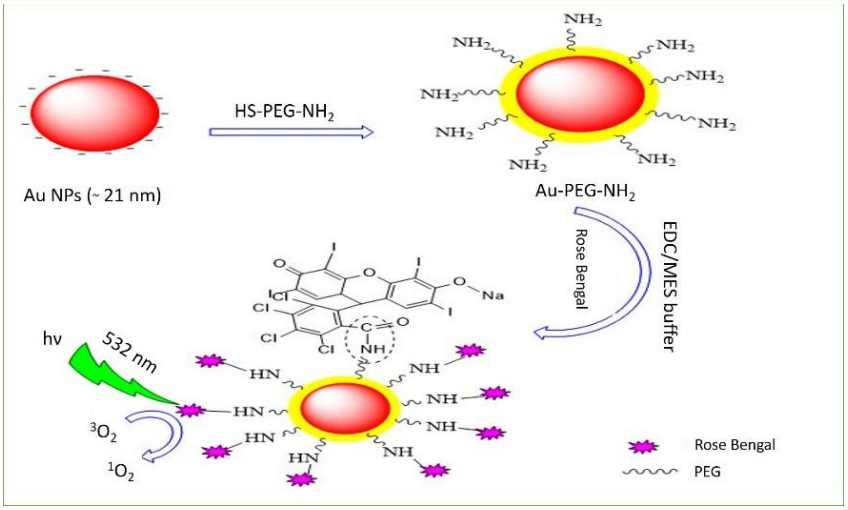

Figure 4.2: The schematic of AuRB conjugate synthesis and singlet oxygen generation mechanism from the conjugate.

4.4 Characterization results

4.4.1 AuNPs

Figure 4.3a shows the UV-Visible absorption spectrum of the Au nanoparticles. The prepared AuNPs were dark red in color due to light scattering which primarily indicates that the particles are small. The as-prepared AuNPs shows the maximum absorption intensity peak at 521 nm. The intensity peak at 521 nm, indicates that the NPs size is less than 20 nm and the absorption curve shape shows that the nanoparticles are uniform in shape [88]. The polydispersity index (PDI) for the AuNPs was observed to be ~0.383 and was suitable for DLS measurements. Figure 4.3b shows the size measurement of the AuNPs using DLS method. The DLS measurement confirms the hydrodynamic size of the AuNPs was ~21.60 nm.

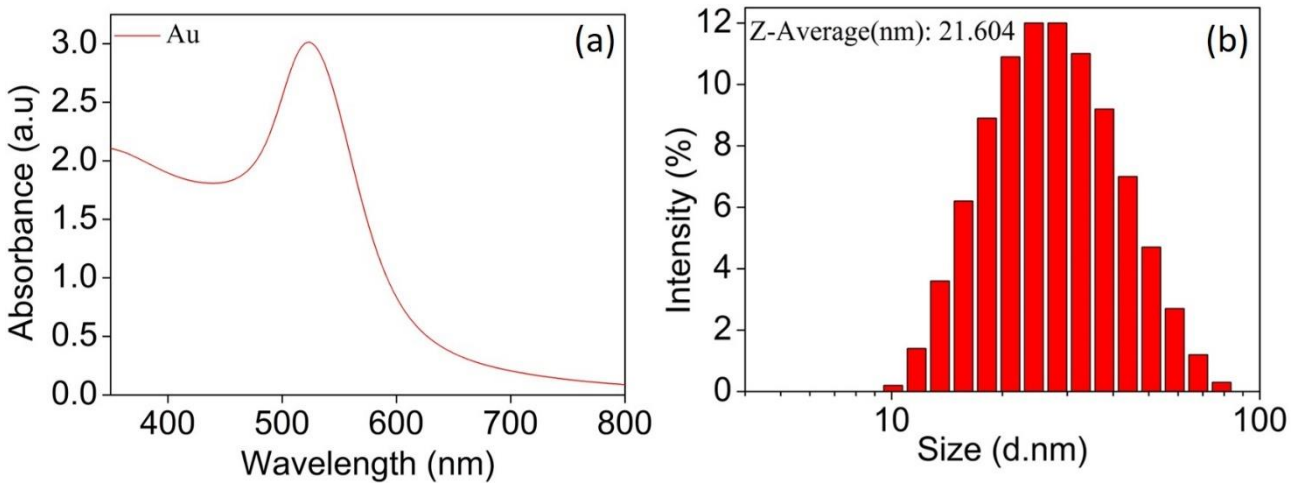

Figure 4.3: (a) Absorption spectra of AuNPs and (b) AuNPs size measured using DLS.

4.4.2 AuRB conjugates

Figure 4.4 compares the absorption spectrum of AuNPs, RB photosensitizer, and AuRB conjugates. The RB photosensitizer without AuNPs conjugation shows the absorption peak at 549 nm. Moreover, the conjugates M1, M2, and M3 show the peak absorption spectra at 568 nm. This means that there is a shift in absorption peak by ~ 19 nm. The change in absorption spectrum is the result of conjugation refractive index of the AuNPs surface due to photosensitizers molecules attached to it. Also, the molecules attached to the AuNPs absorb light close to the plasmon resonance peak due to the plasmonic molecular resonance coupling [89]. The hydrodynamic size measured using DLS for the conjugates M1, M2, and M3 were ~47.63, 47.9, and 48.8 nm, respectively. The Thiol-PEG-NH_2 used to attach of -NH_2 group on nanoparticles surface and the surface functionalization by RB photosensitizer results in increased size of Au nanoparticles.

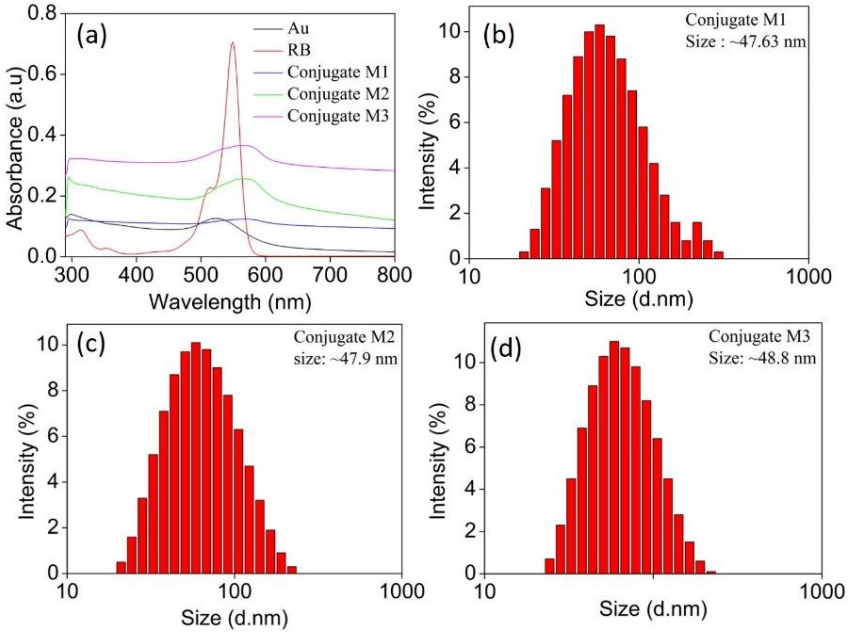

Figure 4.4: (a) UV-Visible absorption spectroscopy of AuRb conjugates, and (b,c,d) shows the DLS size of conjugates M1, M2, M3 respectively.

4.4.3 Surface zeta potential measurements

The measurement of zeta potential allowed to characterize investigated the changes in the surface potential of AuNPs before and after conjugation. The surface charge potential of as-synthesized AuNPs was observed to be ~ -34.9±1.57 mV. The high negatively-charged zeta potential value leads to high a high stability of AuNPs in solution. After functionalization of AuNPs by RB photosensitizer, the surface charge of AuRB conjugate was measured to be ~ -9.875±0.07 nm. The decrease in surface potential is due to the covering of AuNPs by RB molecules. This indicates that RB has successfully conjugated on the surface of Au.

4.5 $^1O_2$ detection using SOSG probe

4.5.1 $^1O_2$ detection from SOSG

In experiments with all the photosensitizers, the 532 nm laser was used for the photosensitization. The laser light was irradiated on the samples for five minutes. The commercially available SOSG probe was used for the detection of $^1O_2$ generated from the photosensitizers. Fluorescence readings were taken by a fluorescence spectrometer every one minute for five minutes. The SOSG probe is reported to be a conjugate of fluorescein and anthracene moieties [83]. Moreover, it has high specificity towards $^1O_2$. So, when photosensitizer generates $^1O_2$ on light irradiation, the SOSG reacts with the anthracene moiety and generates fluorescent EP as shown in figure 4.5a. Ideally, the SOSG probe should not show any fluorescence intensity in the absence of light and any photosensitizer. However, when the fluorescence reading of SOSG in DI water without light irradiation was taken, the SOSG is found to have weak fluorescence emission at 525 nm as showed in figure 4.5b (black). Also, when SOSG in DI water solution was irradiated with 532 nm laser, the SOSG has shown peak intensity at 525 nm wavelength and small increase in the fluorescence emission spectrum with time is may be due to the experimental error or may be due the slight photosensitizing effect of SOSG as illustrated in figure 4.5b. This indicates that the SOSG itself acts as a photosensitizer. In the SOQY calculations, the EPs generated from the SOSG probe is subtracted. This ensures that the $^1O_2$ measured is generated only from photosensitizers and not from the SOSG probe.

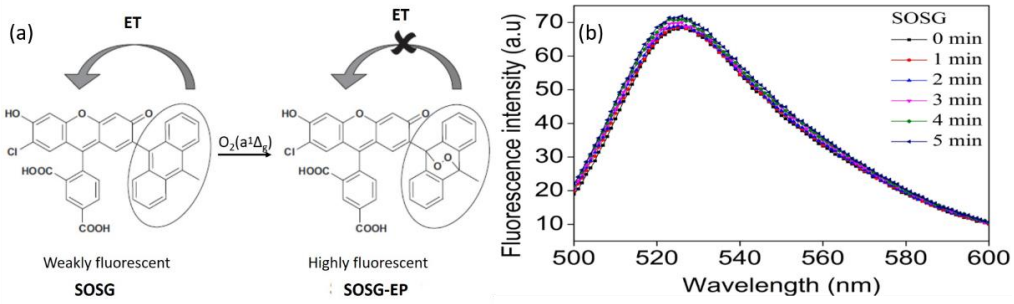

Figure 4.5: (a) Shows the endoperoxides formation of SOSG on reaction with $^1O_2$ generated from photosensitizer. The figure is taken from [90]. (b) Shows the fluorescence emission spectrum of SOSG in DI water.

4.5.2 $^1O_2$ detection from RB

In the first stage, the variation in fluorescence emission verified on RB photosensitizer (0.25 µM, 0.5 µM, and 1 µM) before and after light irradiation. The same SOSG probe from the stock solution was used for detection of $^1O_2$ generated from RB. The RB without light irradiation shows the fluorescence emission spectrum same as the fluorescence spectrum of SOSG-water solution. Figure 4.6 (a, b, and c) shows the emission spectrum of RB before photoirradiation (black). Then with the introduction light on RB, there is a significant increment in fluorescence emission intensity with the irradiation time in RB compared to SOSG in DI water. The RB is sensitive to light and generates $^1O_2$ on light irradiation. The amount of $^1O_2$ generation increases with the increase in laser irradiation time. This $^1O_2$ reacts with the SOSG sensor and creates fluorescent endoperoxides. The fluorescence spectrometer reads the fluorescence emitted from endoperoxides and shows the emission peaks. Figure 4.6 (a, b, and c) shows the fluorescence emission spectrum after photoirradiation on RB. The SOSG fluorescence intensity is plotted against time as shown in figure 4.6d and is used for SOQY calculation in the following sections.

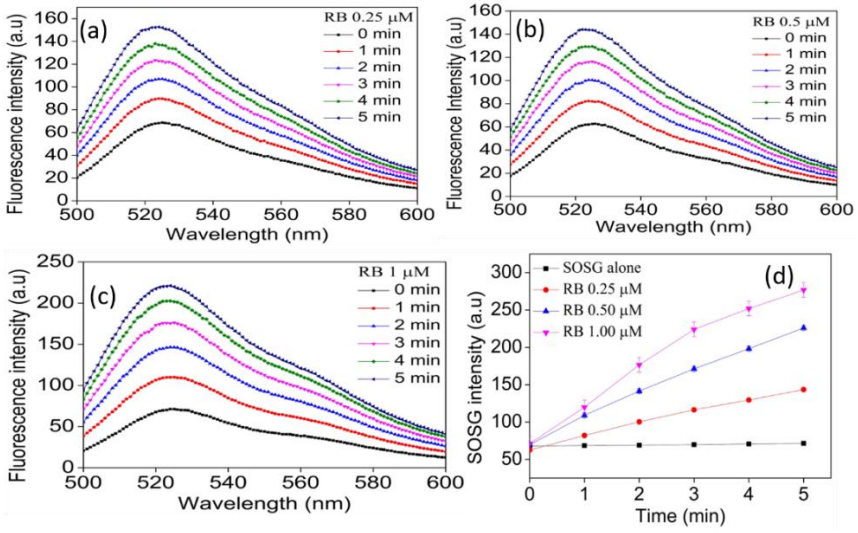

Figure 4.6: Shows the fluorescence intensity spectrum before and after irradiation of 532 nm laser for (a) 0.25 µM RB, (b) 0.50 µM RB (c) 1 µM RB, (d) SOSG fluorescence intensity at 525 nm as a function of time for different concentration of RB and control sample (SOSG).

4.5.3 $^1O_2$ detection in AuNPs

In the second stage, the $^1O_2$ generation and detection experiment was performed on AuNPs with 10 µM, 25 µM, 50 µM concentration. The AuNPs were washed before use. The SOSG detection probe was taken from the same stock solution as the different SOSG vials shows different fluorescence readings. The fluorescence intensity spectrum for AuNPs without laser irradiation is almost same as it was for SOSG-water solution. When light was introduced to the AuNPs, the fluorescence intensity increases with the increase irradiation time as can be seen in figure 4.7 (a, b, c). The AuNPs undergo

surface plasmon resonance when stimulated by the light. Due to plasmon resonance, the absorbed energy is transferred to the surrounding oxygen molecules, and $^1O_2$ is generated. This $^1O_2$ is detected by the SOSG probe and therefore there is an increment in fluorescence spectra as shown in the figure. The SOSG intensity for AuNPs at 525 nm is plotted versus laser irradiation time as illustrated in figure 4.7d. The fluorescence emission for AuNPs is lower compared to RB photosensitizer indicative of low $^1O_2$ generation efficiency. Figure 4.7d is used to measure the SOQY of AuNPs as explained in the subsequent section.

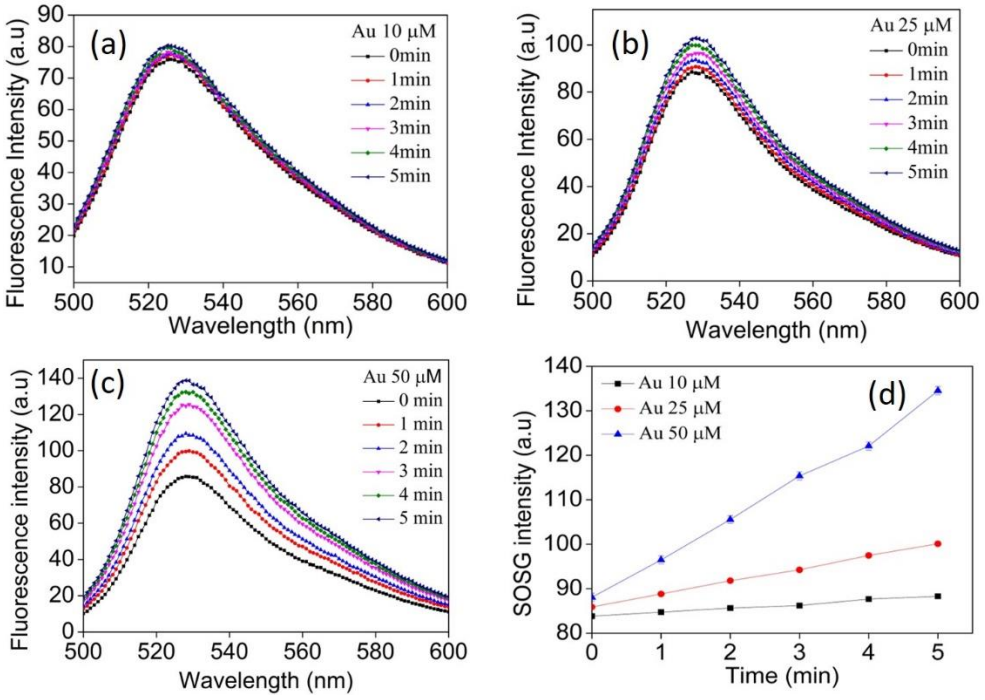

Figure 4.7: Shows the fluorescence intensity spectrum before and after irradiation of 532 nm laser for (a) 10 µM AuNPs (b) 25 µM AuNPs, (c) 50 µM AuNPs (d) SOSG fluorescence intensity at 525 nm as a function of time for different concentration of AuNPs at 525 nm.

4.5.4 $^1O_2$ detection in AuRB

In the final stage, the investigation of $^1O_2$ generation efficiency of AuRB complex conjugates M1, M2, and M3 before and after laser irradiation was carried out. The conjugates M1, M2, and M3 were introduced in water with SOSG probe taken from the same stock solution. The fluorescence emission intensity for all the samples was the same before the introduction of light as shown in figure 4.8 (a, b,c, black). This means there was no $^1O_2$ generation from AuRB conjugates. In this conditions when the conjugates on light irradiation undergo photobleaching. Due to photosensitization, the conjugate molecules excite to the higher electronic state. Moreover, then while returning to its lower excited state release energy. This released energy from conjugate molecules is absorbed by the neighboring oxygen molecules and become excited to its highly reactive singlet state ($^1O_2$). This way the singlet oxygen is generated from the AuRB conjugates. The fluorescence values of the AuRB complex are higher than the RB photosensitizer and AuNPs as shown in figure 4.8(a, b, c). which indicates higher

level $^1O_2$ generated by AuRB conjugates compared to RB and AuNPs. Figure 4.8d shows the SOSG intensity graph of AuRB conjugates plotted against laser irradiation time. Finally, it can be stated from above experiments that in the photosensitization process hydroxyl radicals, superoxide, and nitric oxide may be present but the SOSG sensor does not show any peaks or reaction for these radicals. Also, the SOSG probe is very sensitive to $^1O_2$ detection and demonstrates the increment in fluorescent emission peaks with photoirradiation.

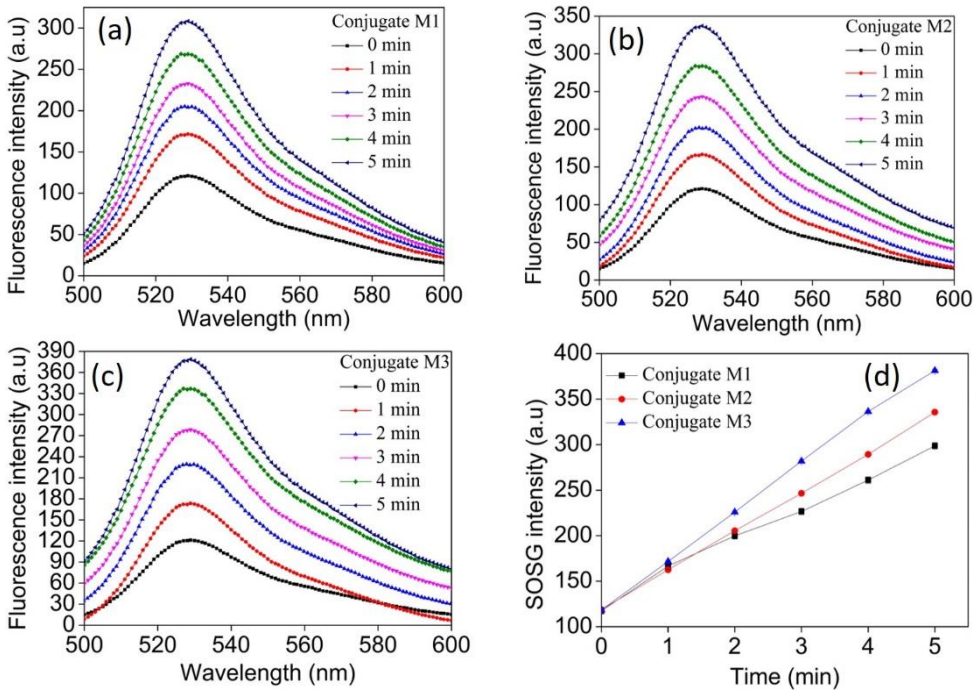

Figure 4.8: Shows the fluorescence intensity spectrum before and after irradiation of 532 nm laser for (a) Conjugate M1, (b) Conjugate M2, (c) Conjugate M3, (d) SOSG fluorescence intensity at 525 nm as a function of time for different concentration of AuRB at 525 nm.

4.5.5 SOQY calculation

The SOSG probe concentrations in every experiment were kept constant at 6 μM as for the SOSG concentration is equal or greater than 6 μM, the reaction order is zero [86]. The rate of reaction for SOSG above 6 μM concentration remains constant [86]. The SOQY of RB is 0.76 [4] and was used as a reference value for the quantum yields calculations. The rate of reaction was obtained from the slope of the SOSG fluorescence intensities of all the samples. Also, as shown in equation 4.4 the term (1-transmittance) for molecular photosensitizers and nanoparticles are the same as the absorption values. The SOQY measurements for AuNPs and AuRB conjugates are described in following sections.

First, we discuss the SOQY measurements for the Au plasmonic nanoparticles. The $^1O_2$ generated from the AuNPs (10 μM, 25 μM, 50 μM) sensitized by 532 nm laser were detected using the SOSG chemiluminescent probe. Figure 4.8a shows the rate of reaction versus β graph for RB

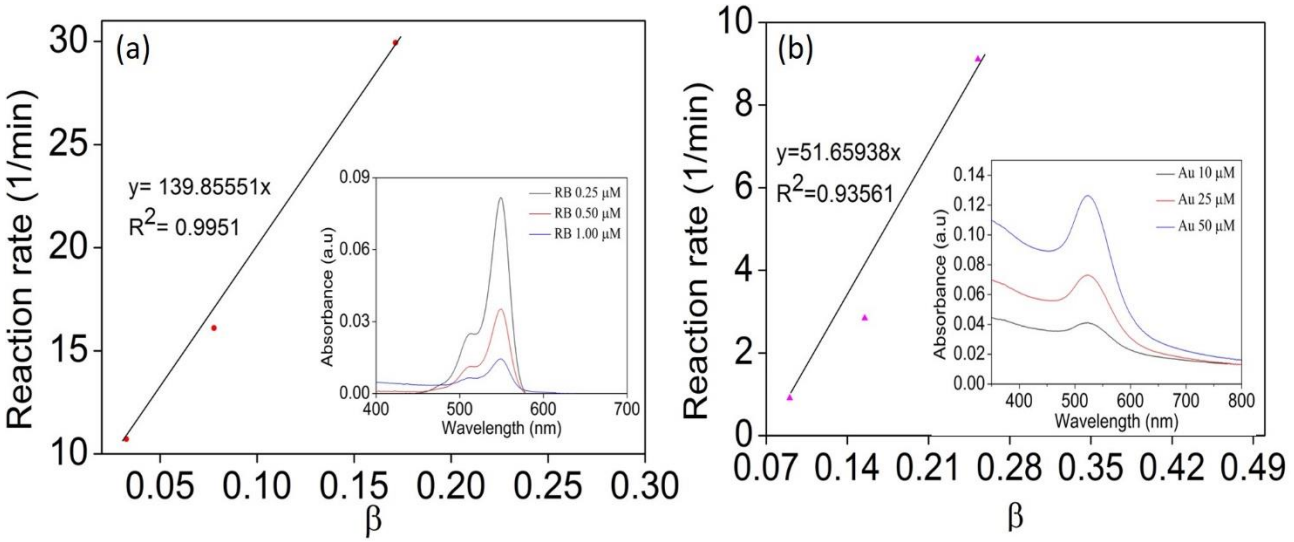

Figure 4.9: (a) Shows the reaction rate vs. β for RB photosensitizer (inset shows the absorbance for RB for 0.25 μM, 0.50 μM, and 1 μM concentration), (b) Shows the reaction rate vs. β for AuNPs (inset shows the absorption spectrum for AuNPs).

photosensitizer. The rate of reaction for RB PS was calculated from the SOSG fluorescent intensity graph illustrated in figure 4.6e. The β (β = 1-transmittance) values were calculated from the absorbance spectra in inset of figure 4.9a. Equation 4.4 was used to calculate the SOQY for AuNPs. Similarly, from the slopes SOSG fluorescence intensities graphs for AuNPs, the reaction rate was calculated shown in figure 4.9b. The reaction rate vs. β plotted is as shown in fig 4.7b. Finally, by using the QY of RB in water as a 0.76 [4] and using the equation 4.6, the QY value calculated for AuNPs was 0.28. This indicates that the Au nanoparticles show certain level of $^1O_2$ generation.

Further, we quantified the SOQY of the metal-photosensitizer covalently conjugated samples M1, M2, and M3. The rate of reaction for AuRB showed in figure 4.10b was calculated from the slope of SOSG fluorescence intensity shown in figure 4.7d. By using the reference QY of RB as 0.76 and equation 4.7, the SOQY for AuRB conjugate was determined to be 0.97±0.0231.

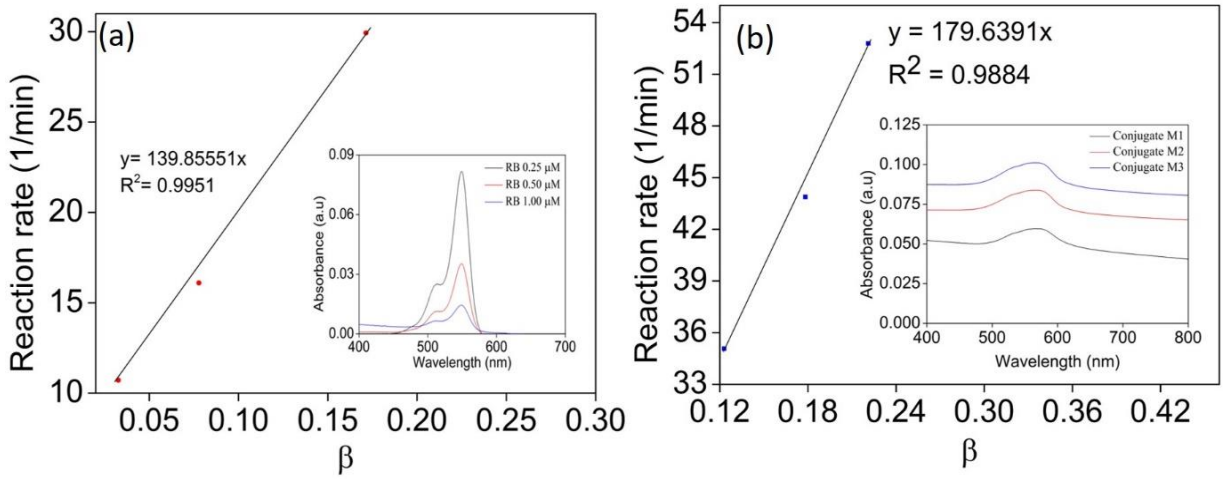

Figure 4.10: (a) Shows the reaction rate vs. β for RB photosensitizer (inset illustrates the absorbance for RB photosensitizer), (b) Shows the reaction rate vs. β for AuRB conjugation (inset shows the absorption spectrum for AuRB).

4.6 Discussion

Metal nanoparticles when irradiated in their plasmon resonance band by the laser light can generate $^1O_2$ [91]. In our case the AuNPs also shown the generation of of small amount $^1O_2$ in light irradiation. The quantum yield of $^1O_2$ generation was very low. The literature reports state that the metal nanoparticles in combination with photosensitizer demonstrates the co-enhancement of fluorescence and of the $^1O_2$ generation [92]. For instance, the silica-coated gold nanorods with silica shell size 2.1 and 28.6 nm when conjugated with aluminum phthalocyanine there was an increase in a co-enhancement factor of 7-fold and 2.1-fold [92]. This indicated that the $^1O_2$ generation efficiency of the photosensitizer molecules attached on the surface of metal nanoparticles changes with their distance from the core nanoparticles We also noticed the similar increase in the SOQY and the enhancement factors due to the existence of metal nanoparticles. Also, it has been reported in the literature study that the metal nanoparticles show electric field enhancement around them when excited with light [87]. Due to this field enhancement in the metal nanoparticles the photosensitizers to absorb the more energy which results in an increase in the $^1O_2$ generation. The $^1O_2$ generation enhancement factor for the AuRB was 1.27. The enhancement factor value of AuRB shows that the localized electric field around the plasmonic AuNPs helped in generating more $^1O_2$ compared to the non-conjugated RB photosensitizer. Also the increase in $^1O_2$ generation could have been due to the enhancement in intersystem crossing and the yield of triplet state [93-94]. This may be due to increased number of singlet excited state of RB. All the above results and observations indicated that the metal nanoparticles in combination with photosensitizer could be a very promising drug in PDT.

Table 2: SOQY and enhancement factor for AuNPs and AuRB conjugates.

Reagents	**SOQY**	**Enhancement factor**
AuNPs	0.28	-
AuRB	0.97±0.0231	1.27

5 Conclusions and future works

5.1 Summary and research outcome

PDT is one of the medically approved cancer treatments. It is based on the idea of delivering the photosensitizer molecule to the tumour tissue. Then the photosensitizer bearing tumour tissues are irradiated by the laser of the appropriate wavelength. On laser absorption, the photosensitizer molecules become excited and transfer energy to the neighboring biomolecules or molecular oxygen. These oxygen molecules then convert from its triplet state to singlet state called singlet oxygen ($^1O_2$) on energy absorption. The $^1O_2$ is highly reactive and kills cancer cells efficiently. The killing of cancer cells in PDT is very specific to the affected cancer cells and do not cause harm to the normal healthy cells. Therefore, this cancer treatment method is non-destructive and to an extent target specific compared to conventional cancer treatment methods.

In this work, we successfully synthesized Au nanoparticles and its conjugates with the different concentrations of RB photosensitizer. I chose 532 nm as the optimum excitation wavelength for the activation of the Au, AuRB conjugates, and RB photosensitizer molecules because the RB photosensitizer shows high absorption at this wavelength range. The photosensitizer samples were irradiated with laser in total for five minutes, and after every one minute, the fluorescence intensity measurement was taken. This procedure was repeated for all the samples of AuNPs, AuRB conjugates, and RB photosensitizer. Singlet Oxygen Sensor Green (SOSG) chemiluminescent probe was used to detect the generated $^1O_2$ on light irradiation. The SOSG on reaction with $^1O_2$ shows green fluorescence emission at around 525 nm. The maximum fluorescence reading was taken at 525 nm for all samples and plotted against wavelength. The slope of these plots gave the rate of reaction

between the SOSG and generated $^1O_2$. Finally, from plots of the rate of reaction and absorption of every sample we calculated the singlet oxygen quantum yield (SOQY).

In concluding the results part, I have successfully synthesized the ~ 21 nm AuNPs of uniform shape. Then the covalent conjugation between AuNPs and different concentration of RB photosensitizer was successful and was confirmed from the UV-Vis absorption measurement. The AuRB conjugation size was ~48 nm. The quantitative measurement of $^1O_2$ showed that the AuNPs generate a small amount of $^1O_2$. The $^1O_2$ generation is may be due to the plasmonic resonance in the AuNPs [92]. This proves that the metal nanoparticles plasmonic effect can help in generating $^1O_2$ which eventually help in increasing the PDT efficacy of the photosensitizer drug.

Finally, AuRB complex conjugates SOQY was 0.97±0.0231. This shows that the AuRB conjugates produce a higher amount of $^1O_2$ than the unconjugated RB (0.76) photosensitizer. Also, it has been reported in the literature that the metal nanoparticles show electric field enhancement around them when excited with the light [87]. The field enhancement in the AuNPs allow the RB PS to absorb more energy which resulted in an increase in the $^1O_2$ generation. The plasmonic resonance effect of AuNPs may have facilitates the increase in $^1O_2$ generation from the photosensitizer molecules. The higher amount of $^1O_2$ generation can have better cytotoxic effect on cancer cells.

5.2 Future work

In this work, I have induced the change in $^1O_2$ generation efficacy of photosensitizer when conjugated with metal nanoparticles. This $^1O_2$ generation effect was studied in an aqueous medium. However, the various nanoparticles size can affect the $^1O_2$ generation efficacy and the actual study on cancer cell samples may have a different effect on $^1O_2$ generation. In the future study, I have two main goals, first is to investigate the effect of a change in nanoparticles size on $^1O_2$ generation efficacy of the photosensitizer and second is to examine the cytotoxic effect of nanoparticles conjugated photosensitizers in vitro.

In the first phase of the future project, the nanoparticles of various metals with different sizes could be synthesized. As discussed in chapter four, the plasmonic effect of metal nanoparticles can help the photosensitizer to increase the $^1O_2$ generation. The surface plasmonic effect changes with a change in the size of the metal nanoparticles. Also, the plasmonic effect is different for different metal nanoparticles. It will be interesting to conjugate various metal nanoparticles of different size to the photosensitizers and then will study the change in $^1O_2$ generation efficacy of photosensitizers. Also, we aim to measure the electric field change around the nanoparticles with size change. Furthermore, the software simulation project to determine the effect of nanoparticles size change on the electric field. Moreover, the electric field enhancement calculated from the experimental results could be compared with the simulations results.

In the second phase of the future project, I will study the cytotoxic effect of metal nanoparticles conjugated photosensitizers effect in vitro on cancer affected cells. First, to achieve this goal, the surface modification of metal nanoparticles will be performed. The nanoparticle surface modification can be carried out by covering the metal nanoparticles in a silica shell or other encapsulating material. Silica is widely used as the shell material because its surface can be modified easily, and it limits the adverse effects of nanoparticles. The silica coated metal nanoparticles surface then can be modified by attaching amine groups, carboxylic groups. Then these modified photosensitizers can be electrostatically or covalently conjugated with the photosensitizers and target ligands. Finally, these nanoparticles conjugated photosensitizer's cytotoxic studies can be performed on cancer cell lines such as squamous carcinoma (4451 cell line), breast cancer (MCF-7), etc. The MTT assay technique will be used on cancer cells to examine the cytotoxic effect.

List of Acronyms/Abbreviations

PDT…… Photodynamic Therapy

ROS…… Reactive Oxygen Species

SOSG…….. Singlet Oxygen Sensor Green

λ_{max}…… Absorption peak wavelength

ε_{max}…… Extintion coefficient

EP……... Endoperoxide

RB…….. Rose Bengal

PS……... Photosensitizer

NIR…… Near Infrared

SPR…… Surface Plasmon Resonance

$^1O_2$……. Singlet Oxygen

UV……. Ultraviolet

NPs…… Nanoparticles

References

[1] Ormond Alexandra, Freeman Harold. "Dye Sensitizers for Photodynamic Therapy." Materials, 1996-1944 63 817.

[2] Pillai, Sreenadh Sasidharan, "Fluorescence Quenching of CdSe/ZnS Quantum Dots by Using Black Hole Quencher Molecules Intermediated With Peptide for Biosensing Application." Cell Medicine 8.1-2 (2015): 57–62. PMC.

[3] Tsay, James M. et al. "Singlet Oxygen Production by Peptide-Coated Quantum Dot-Photosensitizer Conjugates." Journal of the American Chemical Society129.21 (2007): 6865–6871. PMC. Web. 6 Oct. 2016.

[4] Stevens, B.; Ors, J. A.; Pinsky, M. L. Chem. Phys. Lett. 1974, 27, 157.

[5] Ackroyd, R.; Kelty, C.; Brown, N.; Reed, M., "The history of photodetection and photodynamic therapy." Photochem Photobiol 2001, 74 (5), 656-69.

[6] Josefsen, Leanne B., and Ross W. Boyle. "Photodynamic Therapy and the Development of Metal-Based Photosensitisers." Metal-Based Drugs 2008 (2008): 276109.

[7] Moan, J.; Peng, Q.; An outline of the history of PDT. In: T. Patrice, "Photodynamic Therapy. Comprehensive Series in Photochemical and Photobiological Sciences". RSC Publ., London (2003), pp. 3–37.

[8] Sasidharan Swarnalatha Lucky, Khee Chee Soo, and Yong Zhang, "Nanoparticles in Photodynamic Therapy." Chemical Reviews 2015 115 (4), 1990-2042 DOI: 10.1021/cr5004198.

[9] Oleinick, N. L.; Morris, R. L.; Belichenko, I. "The role of apoptosis in response to photodynamic therapy: what, where, why, and how." Photochem. Photobiol. Sci. 2002, 1, 1.

[10] Sharman, W. M.; Allen, C. M.; van Lier, "Role of activated oxygen species in photodynamic therapy" J. E. Methods Enzymol. 2000, 319, 376.

[11] Yavari, N.; Andersson-Engels, S.; Segersten, U.; Malmstrom, P. U. Can. "An overview on preclinical and clinical experiences with photodynamic therapy for bladder cancer." J. Urol. 2011, 18, 5778.

[12] Kostovic, K.; Pastar, Z.; Ceovic, R.; Mokos, Z. B.; Buzina, D. S.; Stanimirovic, A. "Photodynamic therapy in dermatology: current treatments and implications." Coll. Antropol. 2012, 36, 1477.

[13] Allison, R.; Moghissi, K.; Downie, G.; Dixon, K. "Photodynamic therapy (PDT) for lung cancer." Photodiagn. Photodyn. Ther. 2011, 8, 231.

[14] Ana P. Castano, Pawel Mroz & Michael R. Hamblin, "Photodynamic therapy and anti-

tumour immunity". Nature Reviews Cancer 6, 535-545 (July 2006).

[15] Castano, A. P.; Demidova, T. N.; Hamblin, M. R. "Mechanisms in photodynamic therapy: part two-cellular signaling, cell metabolism and modes of cell death." Photodiagn. Photodyn. Ther. 2004, 1, 279.

[16] Plaetzer K.; Krammer B.; Berlanda , "Photophysics and photochemistry of photodynamic therapy: fundamental aspects." J. Lasers Med Sci (2009) 24: 259. Doi:10.1007/s10103-008-0539-1.

[17] Yvette Niamien Konan, Robert Gurny, Eric Allémann, "State of the art in the delivery of photosensitizers for photodynamic therapy." Journal of Photochemistry and Photobiology B: Biology, Volume 66, Issue 2, March 2002, Pages 89-106, ISSN 1011-1344.

[18] Dougherty, T. J., "Studies on the structure of porphyrins contained in Photofrin II." Photochem Photobiol 1987, 46 (5), 569-73.

[19] Dougherty, T. J., "Photodynamic therapy." Photochem Photobiol 1993, 58 (6), 895-900.

[20] Dougherty, T. J.; Gomer, C. J.; Henderson, B. W.; Jori, G.; Kessel, D.; Korbelik, M.; Moan, J.; Peng, Q., "Photodynamic therapy." J Natl Cancer Inst 1998, 90 (12), 889-905.

[21] Ormond, A.; Freeman, H. "Dye Sensitizers for Photodynamic Therapy." Materials 2013, 6(3), 817-840.

[22] D.C Necker "The Indian happiness wart in the development of photodynamic action." Chem. Educ., 1987, 64 (8), p 649. 10.1021/ed064p649.

[23] O. Raab, "Uber die Wirkung fluorescirender Stoffe aur Infusorien.'' Zeitschrift fur Biologie 39, 524-546 (1900).

[24] H. von Tappeiner and A. Jesionek, "Therapeutische Versuche mit fluoreszierenden Stoffen." Munchener medizinische Wochenschrift 47, 2042-2044 (1903).

[25] Lorenzo Brancaleon, H. Moseley; "Laser and Non-laser Light Sources for Photodynamic Therapy." Lasers in Medical Science · February 2002, DOI: 10.1007/s101030200027.

[26] Konig K. "Multiphoton microscopy in life sciences." J Microsc Oxford 2000; 200:83–104.

[27] Deda, Daiana K., & Araki, Koiti. (2015). "Nanotechnology, Light and Chemical Action: an Effective Combination to Kill Cancer Cells." Journal of the Brazilian Chemical Society, 26(12), 2448-2470.

[28] Davis, M. E.; Chen, Z.; Shin, D. M. "Nanoparticle therapeutics: an emerging treatment modality for cancer." Nat. Rev. Drug Discovery 2008, 7, 771.

[29] Reddi, E. "Role of delivery vehicles for photosensitizers in the photodynamic therapy of tumours." J. Photochem. Photobiol. B: Biol. 1997, 37, 189.

[30] Bechet, D.; Couleaud, P.; Frochot, C.; Viriot, M. L.; Guillemin, F.; Barberi-Heyob M.; "Nanoparticles as vehicles for delivery of photodynamic therapy agents." Trends Biotechnol. 2008, 26, 612.

[31] Tomalia, D. A.; Naylor, A. M.; Goddard, W. A. Angew. Chem., Int. Ed. Engl. 1990, 29, 138

[32] Klajnert B, Rozanek M, Bryszewska M, "Dendrimers in photodynamic therapy."Curr. Med Chem. 2012;19(29):4903-12.

[33] Battah, S. H.; Chee, C. E.; Nakanishi, H.; Gerscher, S.; Mac Robert, A. J.; Edwards, C. "Synthesis and biological studies of 5-aminolevulinic acid-containing dendrimers for photodynamic therapy." Bioconjugate Chem. 2001, 12, 980.

[34] Tekade R K.; Kumar P.V; Jain N. K.; "Dendrimers in Oncology: An Expanding Horizon." Chemical Reviews 2009. 109 (1), 49-87.

[35] Kozlowska D, Foran P., MacMohan P., Shelly M.J., Eustace S., O'Kennedy R., "Molecular and magnetic resonance imaging: The value of immunoliposomes." Adv. Drug Deliv, Rev. 2009, 61, 1402-1411.

[36] Bressler N.M.; Bressler S.B. "Photodynamic therapy with verteporfin (Visudyne): Impact of ophthalmology and visual science." Investig. Opthalmol. Vis. Sci. 2000, 41, 624-628.a.

[37] Akbarzadeh, A, Rezaei-Sadabady R, Davaran S, Joo S.W, Zarghami, N, Hanifehpour Y, Samiei M, Kouhi M, Nejati-Koshki K. "Liposome: Classification, preparation, and application." Nanoscale Res. Lett. 2013, 8, 102.

[38] Sadzuka Y.; Iwasaki F.; Sugiyama I.; Horiuchi K.; Hirano T.; Ozawa H.; Kanayama N.; Oku N. Phototoxicity of coproporphyrin as a novel photodynamic therapy was enhanced by liposomalization. Toxicol. Lett. 2008, 182, 110-114.

[39] Sawant, R.R; Torchilin V.P. "Liopsomes as 'smart' pharmaceutical nanocarriers. Soft Matter." 2010,6, 4026-4044.

[40] Nawalany K.; Rusin A.; Kepczynski M.; Mikhailoy A.; Kramer-Marek G.; Snietura M.; Poltowicz J.; Krawczyk Z.; Nowakowska M. Comparison of photodynamic efficacy of tetraarylporphyrin pegylated or encapsulated in liposomes: In vivo studies. J. Photochem. Photobiol. B Biol. 2009, 97, 8-17.

[41] G. Yanyan, R. Snezna, Z. Peng; "Rose Bengal-decorated silica nanoparticles as photosensitizers for inactivation of gram-positive bacteria." Nanotechnology, 21 (2010), p. 065102.

[42] Tewodros Asefa, Zhimin Tao; Biocompatibility of Mesoporous Silica Nanoparticles; Chemical Research in Toxicology 2012 25 (11), 2265-2284 DOI: 10.1021/tx300166u.

[43] Ojea-Jimenez I.; Comenge J.; Garcia-Fernandez L.; Megson Z.A.; Casal E.; Puntes V.F. "Engineered inorganic nanoparticles for drug delivery applications." Curr. Drug Metab. 2013, 14, 518-530.

[44] Ahmed M.Z.; Akhter S.; Jain G.K.; Rahman M.; Pathan S.A.; Ahmad F.J.; Khar R.K. "Metallic nanoparticles: Technology Overview & drug delivery applications in oncology." Expert Opin. Drug Deliv, 2010, 7, 927-942.

[45] Ladj R.; Bitar A.; Eissa M.; Mugnier Y.; Le Dantec. R.; Fessi H.; Elaissari A. "Individual inorganic nanoparticles: Preparation, functionalization and in vitro biomedical diagnostic applications." J. Mater. Chem. B 2013, 1, 1381-1396.

[46] Thienot E.; Germain M.; Piejos K.; Simon V.; Darmon A.; Marill J.; Borghi E.; Levy L.; Hochepied J.F.; Pottier A. "One pot synthesis of new hybrid versatile nanocarriers exhibiting efficient stability in a biological environment for use in photodynamic therapy." J. Photochem. Photobiol. B Biol. 2010, 100, 1-9.

[47] Conde J.; Dias.; Grazu V.; Moros M.; Baptista P.V.; de la Fuente, J.M. "Revisiting 30 years of biofunctionalization and surface chemistry of inorganic nanoparticles for nanomedicine". Front. Chem. 2014, 2, 48.

[48] Guopei Luo, Jiang Long, Bo Zhang, Chen Liu, Shunrong Ji, Jin Xu, Xianjun Yu & Quanxing Ni (2012) "Quantum dots in cancer therapy, Expert Opinion on Drug Delivery." 9:1,47-58.

[49] T. A. Debele; S. Peng.; H. C. Tsai. "Drug carrier for photodynamic cancer therapy." Int. J. Mol. Sci. 2015, 16(9), 22094-22136.

[50] Rizvi S.B.; Ghaderi S.; Keshtgar M.; Seifalian A.M. "Semiconductor quantum dots as fluorescent probes for in vitro and in vivo biomolecular and cellular imaging." Nano. Rev. 2010, 1, 10.3402.

[51] Tsay, James M., Michael Trzoss, Lixin Shi, Xiangxu Kong, Matthias Selke, Michael E. Jung, and Shimon Weiss. "Singlet oxygen production by peptide-coated quantum dot-photosensitizer conjugates." Journal of the American Chemical Society 129, no. 21 (2007): 6865-6871.

[52] Dakrong Pissuwan, Stella M. Valenzuela, Michael B. Cortie, "Therapeutic possibilities of plasmonically heated gold nanoparticles." Trends in Biotechnology, Volume 24, Issue 2, p62–67, February 2006.

[53] Zhang Y.; Aslan K.; Previte, M.J.R., "Metal-enhanced Singlet Oxygen Generation: A Consequence of Plasmon Enhanced Triplet Yields." J Fluoresc (2007) 17: 345.

[54] Yongxia Zhang, Kadir Aslan, Michael J. R. Previte, Chris D. Geddes. "Plasmonic Engineering of singlet oxygen generation." PNAS 2008 105 (6) 1798-1802.

[55] Vankayala, R., Sagadevan, A., Vijayaraghavan, P. Kuo, C.-L.Hwang, K. C. "Metal Nanoparticles Sensitize the Formation of Singlet Oxygen." Angew. Chem. Int. Ed., (2011),50: 10640–10644.

[56] Cheng Yu, Anna C. Samia, Joseph D. Meyers, Irene Panagopoulos, Baowei Fei, Clemens Burda, "Highly efficient drug delivery with gold nanoparticle vectors for in vivo photodynamic therapy of cancer." Journal of the American Chemical Society 130, no. 32 (2008): 10643-10647.

[57] Jiasjing Yu, Che-Hao Hsu, Chih-Chia Huang, Po-Yang Chang. "Development of Therapeutic Au–Methylene Blue Nanoparticles for Targeted Photodynamic Therapy of Cervical Cancer Cells." ACS Appl. Mater. Interfaces, 2015, 7 (1), pp 432–441.

[58] Zhao, Linlin, Tae-Hyun Kim, Hae-Won Kim, Jin-Chul Ahn, and So Yeon Kim. "Surface-enhanced Raman scattering (SERS)-active gold nanochains for multiplex detection and photodynamic therapy of cancer." Acta biomaterialia 20 (2015): 155-164.

[59] R. Dosseli, C. Tampieri, R. Ruiz-González, S. DeMunari, X. Ragàs, D. Sánchez-García, M. Agut, S. Nonell, E. Reddi, M.Gobbo, "Synthesis, characterization, and Photoinduced antibacterial activity of porphyrin-type photosensitizers conjugated to the antimicrobial peptide apidaecin1b." J. Med. Chem. 56 (2013) 1052–1063.

[60] X. Chen, L. Hui, D. A. Foster, C. M. Drain, "Efficient Synthesis and photodynamic activity of porphyrin–saccharide conjugates: targeting and incapacitating cancer cells." Biochemistry 43 (2004) 10918–10929.

[61] Liuen Liang, Andrew Care, Run Zhang, Yiqing Lu, Nicolle H. Packer, Anwar Sunna, Yi Qian, and Andrei V. Zvyagin, "Facile Assembly of Functional Upconversion Nanoparticles for Targeted Cancer Imaging and Photodynamic Therapy." ACS Applied Materials & Interfaces 2016 8 (19), 11945-11953.

[62] Guofeng Wang, Qing Peng, and Yadong Li, "Lanthanide-Doped Nanocrystals: Synthesis, Optical-Magnetic Properties, and Applications." Accounts of Chemical Research 2011 44 (5), 322-332.

[63] Ruichan Lv, Dan Yang, Piaoping Yang, Jiating Xu, Fei He, Shili Gai, Chunxia Li, Yunlu Dai, Guixin Yang, and Jun Li, "Integration of Upconversion Nanoparticles and Ultrathin Black Phosphorus for Efficient Photodynamic Theranostics under 808 nm Near-Infrared Light Irradiation." Chemistry of Materials 2016 28 (13), 4724-4734.

[64] D. Yang, P. Ma, Z. Hou, Z. Cheng, C. Li and J. Lin, "Current advances in lanthanide ion (Ln^{3+})-based upconversion nanomaterials for drug delivery." Chem. Soc. Rev., 2015, 44, 1416.

[65] M. E. Lim, Y. Lee, Y. Zhang, J. J. H. Chu, "Photodynamic inactivation of viruses using upconversion nanoparticles." Biomaterials 2012, 33, 1912.

[66] Dongmei Yang, Ping'an Ma, Zhiyou Hou, Ziyong Cheng, Chunxia Li, and Jun Lin, "Current advances in lanthanide ion (Ln3+)-based upconversion nanomaterials for drug delivery." Chem. Soc. Rev., DOI: 10.1039/c4cs00155a.

[67] G. Yu, Y. Shan, G. C. Li, K.Z. Chen, "Synthesis and characterization of bifunctional magnetic optical Fe3O4@SiO2@Y2O3: Yb3+, Er3+ near-infrared-to-visible up-conversion nanoparticles." J. Mater CHem., 2011,21, 8104-8109.

[68] Y. Wang, P.P. Yang, P. A. Ma, F.Y Qu, S. L. Gai, N. Niu, F. He, "Hollow structured $SrMoO_4$:Yb^{3+}, Ln^{3+} (Ln = Tm, Ho, Tm/Ho) microspheres: tunable up-conversion emissions and application as drug carriers." J. Lin. J. Mater. Chem. B, 2013, 1, 2056-2065.

[69] J. Liu, F. Liu, K. Gao, J. S. Wu and D. F. Xue, J. "Recent developments in the chemical synthesis of inorganic porous capsules." J Mater Chem 2009, 19: 6073–6084. 10.1039/b900116f'. Mater. Chem., 2009, 19, 6073–6084.

[70] C. Wang, L. Cheng and Z. Liu, "Drug delivery with upconversion nanoparticles for multi-functional targeted cancer cell imaging and therapy." Biomaterials, 2011, 32,1110–1120.

[71] B. Dong, H. W. Song, H. Q. Yu, H. Zhang, R. F. Qin, X. Bai, G. H. Pan, S. Z. Lu, F. Wang, L. B. Fan and Q. L. Dai, "Remarkable enhancement of upconversion fluorescence and confocal imaging of PMMA Opal/$NaYF_4$:Yb^{3+}, Tm^{3+}/Er^{3+} nanocrystals." J. Phys. Chem. C, 2008, 112, 1435–1440.

[72] N. M. Idris, M. K. Gnanasammandhan, J. Zhang, P. C. Ho, R. Mahendran, Y. Zhang, "Near infrared light-mediated photoactivation of cytotoxic Re(I) complexes by using lanthanidedoped upconversion nanoparticles." Nat. Med. 2012, 18, 1580.

[73] Ttp://photobiology.info/Berg.html.

[74] Bo Zhao, Tianyou Zhang, Bei Chu, Wenlian Li, Zisheng Su, Hairuo Wu, Xingwu Yan, Fangming Jin, Yuan Gao, Chengyuan Liu; "Highly efficient red OLEDs using DCJTB as the dopant and delayed fluorescent exciplex as the host." Scientific Reports 5, 10.1038/srep10697.

[75] Joseph R. Lakowicz, "Principles of fluorescence spectroscopy." edition ISBN-13: 978-0387-31278-1.

[76] Skoog, Holler, Crouch, "Principles of Instrumental Analysis." 6th edition, ISBN-13: 978-0495012016 ISBN-10: 0495012017.

[77] Kaszuba, Michael, et al. "High-Concentration Zeta Potential Measurements Using Light-Scattering Techniques." Philosophical transactions. Series A, Mathematical, physical, and engineering sciences 368.1927 (2010): 4439–4451. PMC. Web. 1 Sept. 2016.

[78] T. Breitenbach, M. K. Kuimova, P. Gbur, S. Hatz, N. B. Schack, B. W. Pedersen, J. D. C. Lambert, L. Poulsen and P. R. Ogilby, "Photosensitized production of singlet oxygen: spatially-resolved optical studies in single cells." Photochem. Photobiol. Sci., 2009, 8, 442.

[79] I. Zebger, J. W. Snyder, L. K. Andersen, L. Poulsen, Z. Gao, J. D. C. Lambert, U. Kristiansen and P. R. Ogilby, "Direct Optical Detection of Singlet Oxygen from a Single Cell." Photochem. Photobiol., 2004, 79, 319–322.

[80] https://tools.thermofisher.com/content/sfs/manuals/mp36002.pdf, Singlet Oxygen Sensor Green Reagent.

[81] Ragas, X.; Jimenez-Banzo, A.; Sanchez-Garcia, D.; Batllori, X.; Nonell, S.; "Singlet Oxygen Photosensitisation by the Fluorescent Probe Singlet Oxygen Sensor Green." Chem. Commun. 2009, 2920−2922.

[82] Gollmer, A.; Arnbjerg, J.; Blaikie, F.; Pedersen, B.; Breitenbach, T.; Daasbjerg, K.; Glasius, M.; Ogilby, P. "Singlet Oxygen Sensor Green: Photochemical Behavior in Solution and in a Mammalian Cell." Photochem. Photobiol. 2011, 87, 671−679.

[83] Kim S, Fujitsuka M, Majima, "The Photochemistry of singlet oxygen sensor green." J Phys Chem B. 2013 Nov 14;117(45):13985-92.

[84] Tanaka, K.; Miura, T.; Umezawa, N.; Urano, Y.; Kikuchi, K.; Higuchi, T.; Nagano, T. "Rational Design of Fluorescein-Based Fluorescence Probes. Mechanism-Based Design of a Maximum Fluorescence Probe for Singlet Oxygen." J. Am. Chem. Soc. 2001, 123, 2530−2536.

[85] You Qiu He, Shao Pu Liu, Ling Kong, Zhong Fang Liu, "A study on the sizes and concentrations of gold nanoparticles by spectra of absorption, resonance Rayleigh scattering and resonance non-linear scattering, Spectrochimica Acta Part A: Molecular and Biomolecular Spectroscopy." Volume 61, Issues 13–14, October 2005, Pages 2861-2866, ISSN 1386-1425.

[86] Lin, H., Shen, Y., Chen, D.; "Feasibility Study on Quantitative Measurements of Singlet Oxygen Generation Using Singlet Oxygen Sensor Green." J Fluorescence (2013) 23: 41. doi:10.1007/s10895-012-1114-5.

[87] Sandhya Clement, Mushtaq Sobhan, Wei Deng, Elizabeth Camilleri, Ewa M. Goldys, "Nanoparticle-mediated singlet oxygen generation from photosensitizers." Journal of Photochemistry and Photobiology A: Chemistry, Volume 332, 1 January 2017, Pages 66-71, ISSN 1010-6030.

[88] http://www.cytodiagnostics.com/store/pc/Introduction-to-Gold-Nanoparticle-Characterization-d3.html.

[89] J.-H. Wang, B. Wang, Q. Liu, Q. Li, H. Huang, L. Song, T.-Y. Suna, H. Wang, X.-F. Yua, C. Li, and P. K. Chu; "Bimodal optical diagnostics of oral cancer based on Rose Bengal conjugated gold nanorod platform." Biomaterials 34, 4274 (2013).

[90] Tobias Kiesslich, Anita Gollmer, Tim Maisch, Mark Berneburg, and Kristjan Plaetzer, "A Comprehensive Tutorial on In Vitro Characterization of New Photosensitizers for Photodynamic Antitumor Therapy and Photodynamic Inactivation of Microorganisms." BioMed Research International, vol. 2013, Article ID 840417, 17 pages, 2013. doi:10.1155/2013/840417.

[91] Samantha J. Chadwick, Dina Salah, Penelope M. Livesey, Mathias Brust, and Martin Volk, "Singlet Oxygen Generation by Laser Irradiation of Gold Nanoparticles." The Journal of Physical Chemistry C 2016 120 (19), 10647-10657

[92] Ke, Xuebin, et al. "Co-Enhancement of Fluorescence and Singlet Oxygen Generation by Silica-Coated Gold Nanorods Core-Shell Nanoparticle." Nanoscale Research Letters 9 (2014): 666. PMC. Web. 7 Oct. 2016.

[93] Cheng YC, Samia A, Meyers JD, "Panagopoulos I, Fei B, Burda C. "Highly efficient drug delivery with gold nanoparticle vectors for in vivo photodynamic therapy of cancer." J Am Chem Soc. 2008;130:10643–10647.

[94] Zhang Y, Aslan K, Previte MJ, Geddes CD. "Metal-enhanced singlet oxygen generation: a consequence of plasmon enhanced triplet yields." J Fluoresc. 2007;17:345–349. doi: 10.1007/s10895-007-0196-y.